



Ionic Liquid Hydrogels Based on Poly(2-acrylamido-2-methyl-1-propanesulfonic Acid -*co*-1-vinylimidazole): A Green and Efficient Catalyst Carrier for Ag Nanoparticles in Oxidation and Adsorption of Benzyl Alcohol in Water

Hamidreaz Mohammadi¹ · Massomeh Ghorbanloo¹ · Masami Mori² · Hidenori Yahiro²

Received: 5 March 2022 / Accepted: 2 July 2022 / Published online: 22 July 2022
© The Author(s), under exclusive licence to Springer Science+Business Media, LLC, part of Springer Nature 2022

Abstract

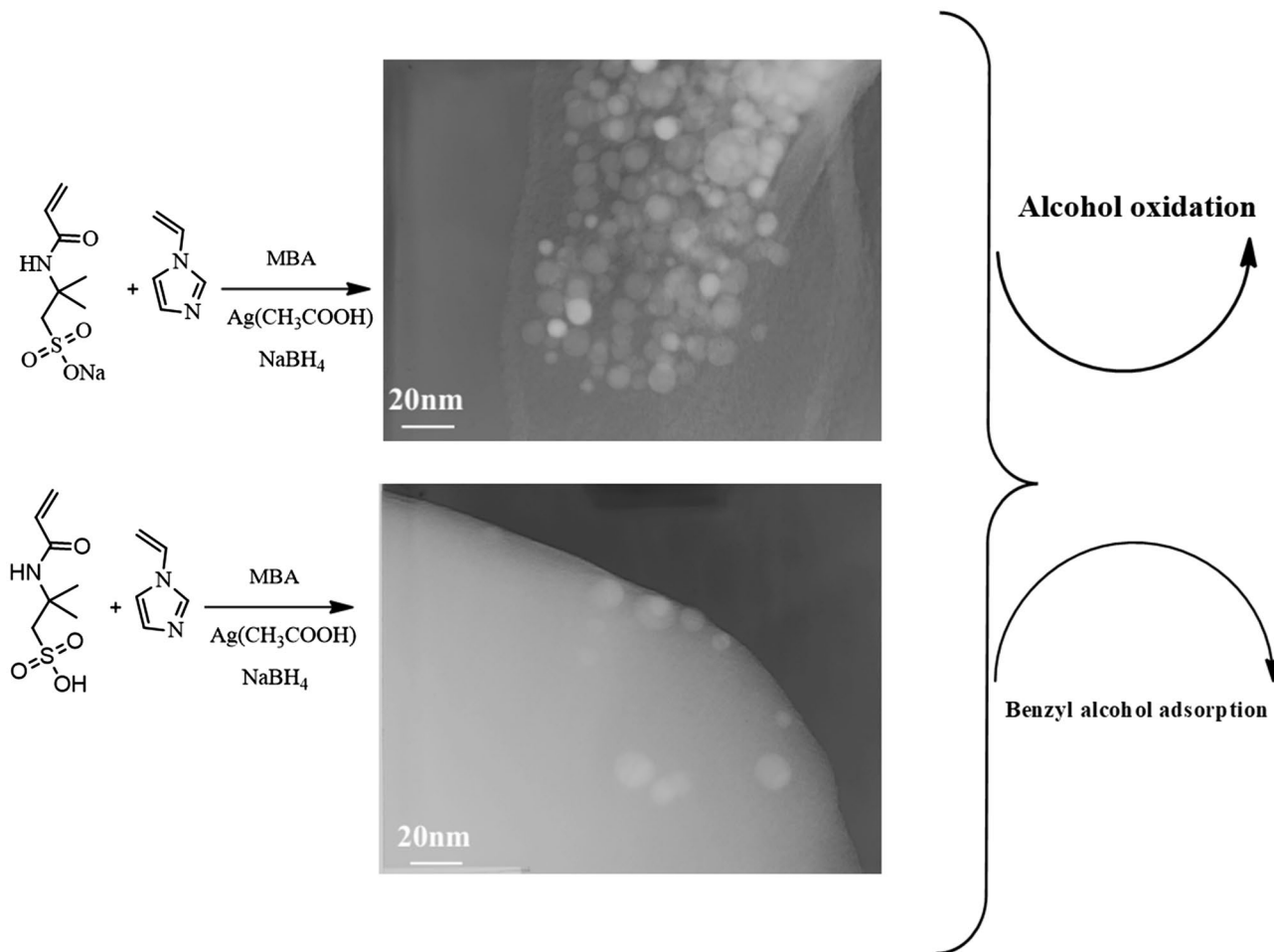
Radical polymerization reactions were employed to synthesize poly(2-acrylamido-2-methyl-1-propanesulfonic acid -*co*-1-vinylimidazole), hydrogels at neutral and acidic reaction conditions. The results of Fourier Transform Infrared (FT-IR) spectroscopy and scanning electron microscopy spectroscopy confirmed the chemical composition of the synthesized hydrogels. Loading Ag into hydrogels, removing loosely-bound Ag ions, and reducing Ag ions with sodium borohydride (NaBH₄) were used to construct p(AMPS-Na⁺-*co*-VIm)-Ag and p(AMPS-H⁺-*co*-VIm)-Ag. Metal nanoparticles embedded p(AMPS-Na⁺-*co*-VIm)-Ag and p(AMPS-H⁺-*co*-VIm)-Ag were visualized by high resolution X-ray photoelectron spectroscopy, transmission electron microscopy and energy dispersive X-ray. FT-IR spectroscopy and HR-XPS demonstrated that the interaction of network heteroatoms with Ag nanoparticles was responsible for stabilizing silver nanoparticles. Atomic absorption spectroscopy was also employed to measure the concentrations of metals in all compounds. P(AMPS-Na⁺-*co*-VIm)-Ag and p(AMPS-H⁺-*co*-VIm)-Ag composites were used as catalyst in the oxidation of alcohols by emphasizing the effects of different parameters such as oxidant, substituent effect, etc. The prepared porous hydrogels and related composites were also utilized in the adsorption of Benzyl alcohol from aqueous solutions. P(AMPS-Na⁺-*co*-VIm) and its composite has better performance than p(AMPS-H⁺-*co*-VIm) and p(AMPS-H⁺-*co*-VIm)-Ag. Because, absorption capacity is increased with an increase in the high porosity and it is depending on porous size and shapes. In continue, quaternization effect by 1,4-dibromobutane on catalytic performance of nano-composites was investigated. The results confirmed the easy separation of the prepared catalysts from the reaction media. Moreover, the catalysts could efficiently be recycled four times without losing their quality. It was also proved that the catalysts were recyclable, durable, and leaching-resistant.

✉ Massomeh Ghorbanloo
m_ghorbanloo@znu.ac.ir; m_ghorbanloo@yahoo.com

¹ Department of Chemistry, Faculty of Science, University of Zanjan, Zanjan 45371-38791, Iran

² Department of Materials Science and Biotechnology, Graduate School of Science and Engineering, Ehime University, Matsuyama 790-8577, Japan

Graphical Abstract



Keywords 1-Vinylimidazole · 2-Acrylamido-2-methyl-1-propane sulfonic acid · Benzyl alcohol adsorption · Oxidation · Quaternization

1 Introduction

Hydrogels, as three-dimensional (3D) cross-linked polymer networks, have received tremendous attention in chemistry since they offer a number of benefits owing to their unique physical and chemical characteristics. These networks possess various pore sizes, large surface areas, great biocompatibility, high water absorption capacity, great capabilities of ion transport, adjustable mechanical properties, high permeability, hydrophilicity, and thermal stability. Other advantages of these networks are excellent flexibility with respect to swelling kinetics and quick diffusion processes. Moreover, their surface properties are changeable. For instance, the surface area can be charged either positively or negatively. Their acid/base characteristics are also excellent [1, 2]. These features make hydrogels promising materials for

various applications in different industries, including food technology, water resource engineering, agricultural engineering, and biomedical engineering [3–5].

In many types of hydrogels, the ionic liquids (ILs) based hydrogels which means that the gel contains ILs are attractive [6]. ILs are comprised of organic cations and inorganic anions and are employed to prepare some gels. As polymer chains, poly(ionic liquid)s (PILs) composed of repeating units of ILs monomers. These polymer chains possess unique features because they inherit the great attributes of ILs. For instance, the thermal stability and ionic conductivity of PILs are excellent and their electrochemical window is wide. PILs have not only the attributes of ILs (e.g., viscoelastic features) but also the inherent characteristics of polymer (e.g., high versatile processability, mechanical stability, facile functionalization, thermal stability, flexibility,

and durability) [7]. Therefore, compared to ILs, PILs are more suitable materials with greater efficiency. Over the past years, PILs have emerged as one of the hottest interdisciplinary topics in polymer sciences, materials sciences, catalysis, separation, analytical chemistry, cell biology, and electrochemistry [8, 9].

Owing to the softness, flexibility, and versatility of the 3D network structure of poly(ionic liquid)-based hydrogels and the adjustability and simplicity of their chemical and physical features, they are considered appropriate candidates for immobilizing catalytic enzymes and catalytic inorganic nanoparticles [10, 11]. Possessing the specific properties of both hydrogels and metal nanoparticles (NPs), poly-ionic hydrogels primarily function as carriers of NPs. The outstanding chemical and physical properties of poly-ionic hydrogels facilitate the uniform distribution of NPs and prepare a suitable environment for various reactions, especially aqueous-phase catalysis. By using these hydrogels, the permeability of metal into gels is promoted. The special chemical structure of poly-ionic hydrogel plays important role in the absorption of metal ion into the gel, and further in the control of nanoparticle size as well as prevention of their agglomeration during the in situ preparation and even application process of NPs.

These robust nanocomposites not only have the great attributes of polymers (*e.g.*, good stability and reusability) but also possess great properties of NPs (*e.g.*, optical, magnetic, electric, and biological features). Due to the increasing importance of sustainable development in chemistry and the chemical industry, numerous researchers have devoted their attention to production processes and focused on finding effective ways to implement the principles of Green Chemistry [12].

In industrial sustainability, a critical issue is treatment of wastewater. Since green nanomaterials attracted a lot of attention to play a crucial role in water treatments with high surface-to-volume ratios, great porosity, and large and quick removal rates as environmentally friendly adsorbents of water pollution [13]. However, in order to purify and desalinate water via these nanomaterials, scientists have encountered a number of challenges as these nanomaterials are toxic and some environmental regulations restrict their use. For the purification of wastewater from toxic organic and inorganic pollutants, countless green nanomaterials, including, noble metal nanoparticles (*e.g.*, gold and silver), metal oxides (*e.g.*, ferric oxides and manganese oxides), carbon nanotubes, graphene, and nanocomposites, have been introduced [13].

The current study aims to propose a simple and scalable way to construct noble metal nanoparticles, *i.e.*, catalytically active metallic silver, in situ using vinyl imidazole-based hydrogels. One of the critical concerns in this process is to promote the swelling of hydrogels and their absorption

capacity of metal ions. To address this issue, VIm has been copolymerized with hydrophilic monomers, having metal ion absorbing tendencies such as AMPS- Na^+ and AMPS- H^+ .

In this context, the current work was designed to explore the potential of p(AMPS- Na^+ -*co*-VIm), p(AMPS- H^+ -*co*-VIm) and 1,4-BB-p(AMPS- Na^+ -*co*-VIm) bulk hydrogel in the fabrication of metal nanoparticles and subsequently as reactor media and catalyst in catalytic reactions. The resultant Ag-nanocomposites catalysts, show an excellent catalytic performance for the oxidation of alcohols and adsorption of benzyl alcohol from aqueous media. More interestingly, the p(AMPS- Na^+ -*co*-VIm) catalyst can be easily separated after catalytic reaction and readily recycled over four successive reaction cycles. Since the eco-friendly and inexpensive p(AMPS- Na^+ -*co*-VIm) is catalytically effective with superior recyclability.

2 Experimental Section

2.1 Materials and Equipment

The monomers, 2-acrylamido-2-methyl-1-propanesulfonic acid (AMPS- H^+) and 2-acrylamido-2-methylpropane sulfonic acid sodium salt (AMPS- Na^+) solution 50%, as ionic monomer (98%, Sigma Aldrich), 1-Vinylimidazole (1-VIm) (99%, Sigma Aldrich) as monomers, the crosslinker, N, N'-methylenebisacrylamide (MBA) (99%, Across), the initiators, 2,2'-azobis(isobutyronitrile) (AIBN) (99%, Sigma Aldrich) and the accelerator N,N,N',N'-tetramethylmethylenediamine (TEMED) (98% Across) were used in hydrogel preparation. Ag(CH_3COO) (Merck) was used as metal ion source. Sodium borohydride (NaBH_4 , 98%, Merck) was used in the reduction of metal ions to prepare metal nanoparticles. All the chemicals were used as received without further purification. FT-IR spectra were recorded in KBr disks with a Bruker FT-IR spectrophotometer. The exact amount of the silver in the composites was determined by Varian Spectra 220 AA spectroscopy. Morphology of swollen p(AMPS-*co*-VIm) and p(NaAMPS-*co*-VIm) hydrogels was investigated with Scanning Electron Microscopy (SEM) via MIRA3 TESCAN FE SEM and an accelerating voltage of 10 keV. The sample was swollen and quickly frozen in liquid nitrogen. The hydrogel was freeze-dried at $-50\text{ }^\circ\text{C}$ for 3 days to preserve their porous structure without any collapse. After that, the dried samples were deposited onto an aluminum stub and sputter-coated with gold for 60 s to enhance conductivity. Transmission electron microscopy (TEM, PHILIPS CM-30) was used to find out the size of metal nanoparticles inside the hydrogel nanocomposites. Particles in ethanol was sonicated and 5 μL suspension immediately transferred to Cu grids completely covered with carbon, and dried under room conditions. They

were analyzed in a Jeol 200 keV field emission transmission electron microscopy and electron diffraction data were supported by EDS obtained on single nanoparticles. The high resolution X-ray photoelectron spectrum (HRXPS) was performed by a 1600E Perkin Elmer applying Mg-K α excitation source. The reaction products of oxidation were determined and analyzed using an HP Agilent 6890 gas chromatograph equipped with a HP-5 capillary column (phenyl methyl siloxane 30 m \times 320 μ m \times 0.25 μ m).

2.2 Preparation of Hydrogels

2.2.1 Neutral Reaction Solution

Free-radical polymerization reaction techniques were used to synthesize polymeric hydrogels at 65 °C. In this process, 0.16 mL (0.85 mmol) of AMPS-Na⁺ and 0.03 mL (0.36 mmol) 1-VIm monomers were initially combined. Then, 0.015 g (5% monomer, 0.1 mmol) MBA and 50 μ L TEMED as crosslinking agent and accelerator, respectively, were added to the mixture. With the addition of 0.0075 g (10% monomer, 0.045 mmol) AIBN in 0.75 mL ethanol to the prepared mixture, polymerization reactions started. The resulting solution was placed in plastic straws for four hours at 65 °C so that the polymerization reactions were completed.

Selected FT-IR (KBr, cm⁻¹): (p(AMPS-Na⁺-co-VIm)): 3450 (br, s), 3107 (shoulder), 2989 (w), 2933 (w), 1662 (vs), 1547 (s), 1393 (m), 1372 (w), 1302 (w), 1225 (m), 1193 (w), 1161 (w), 1119 (m), 1087 (w), 1051 (s), 915 (w), 862 (w), 819 (w), 766 (w), 670 (w), 627 (m), 531 (w).

2.2.2 Acidic Reaction Solution

In the synthesis of p(AMPS-H⁺-co-VIm) hydrogels, 0.124 g (0.6 mmol) AMPS, 0.054 mL (0.6 mmol) 1-VIm, 0.015 g (5% monomer, 0.1 mmol) MBA and 50 μ L TEMED were mixed with 0.5 mL ethanol and to this solution a separately prepared AIBN solution of 0.005 g (5.5% monomer, 0.033 mmol) AIBN in 0.25 mL ethanol was added and vortexed homogeneously, as shown in Scheme 1. The mixture was placed into plastic straws (~4 mm in diameter), and these plastic straws were immersed in a 65 °C water bath for 4 h to complete polymerization and crosslinking. The mixture was transferred to plastic straws (~4 mm in diameter), and kept as such for 4 h at 65 °C to complete polymerization and crosslinking. Finally, the obtained 3-D hydrogels were kept submersed in water for 24 h. After the cleaning procedure, hydrogels were dried in an oven at 40 °C till constant weight.

Selected FT-IR (KBr, cm⁻¹): (p(AMPS-H⁺-co-VIm)): 3529 (br, s), 3129 (w), 3065 (w), 2979 (w), 2937 (w), 2862 (w), 1662 (s), 1544 (s), 1463 (m), 1393 (w), 1369 (w),

1305 (m), 1230 (w), 1187 (w), 1155 (w), 1113 (w), 1091 (m), 1037 (vs), 908 (w), 854 (w), 822 (w), 769 (m), 664 (w), 625 (s), 523 (w), 459 (w).

2.3 In Situ Synthesis of Metal Nanoparticles Within p(AMPS-H⁺-co-VIm) and p(AMPS-Na⁺-co-VIm) Hydrogels

Ultimately, the obtained hydrogels were immersed in the aqueous medium. By using the impregnation-reduction method in water, a number of Ag nanoparticles were loaded into the p(AMPS-H⁺/AMPS-Na⁺-co-VIm) hydrogels. Subsequently, p(AMPS-H⁺/AMPS-Na⁺-co-VIm) (0.25 g) was submerged in the aqueous solution of Ag (CH₃COO) (500 ppm) and stirred unceasingly. The next step involved the filtration and wash of the hydrogels including metal ions with water. The purpose of this step was to eliminate silver ions with loose bonds. Afterward, NaBH₄ was used to reduce silver ions on the hydrogels. Then, deionized water was employed to filter and wash the obtained Ag catalyst.

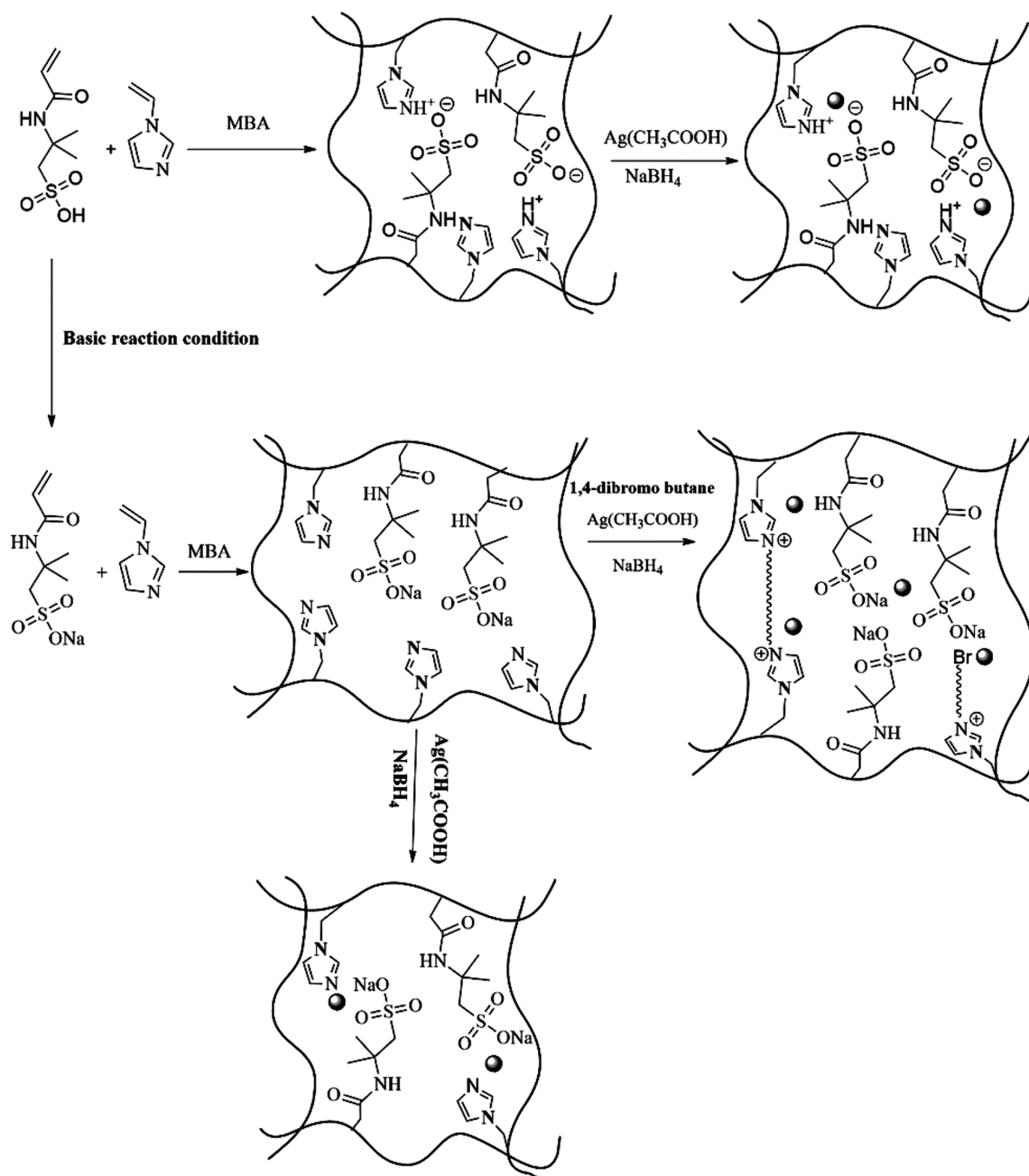
2.4 Swelling Behavior of p(AMPS-H⁺-co-VIm) and p(AMPS-Na⁺-co-VIm) Hydrogels

The swelling experiments for the both hydrogels were carried out in water (at room temperature). Pre-weighted hydrogels were immersed in any of the aforementioned solvents and the mass increase was recorded by weighing the soaked hydrogels at certain time intervals after blot drying with filter paper to remove the excess solvent on the surface.

2.5 Quaternization of Hydrogel

To create a positive charge on p(AMPS-Na⁺-co-VIm) hydrogels, the modification agent, 1,4-BB were reacted with p(AMPS-Na⁺-co-VIm) hydrogels, as shown in Scheme 1. In the quaternization reaction, about 0.1 g dried hydrogels were treated with 1,4-BB (0.56 mL) in 20 mL ethanol mixtures at 50 °C at 200 rpm mixing rate for 24 h. Then the quaternized hydrogels were washed with plenty of acetone to remove the unreacted reactants from the hydrogel matrices and finally, quaternized p(AMPS-Na⁺-co-VIm) hydrogels, (Q- p(AMPS-Na⁺-co-VIm)), were dried in an oven at 40 °C.

Selected FT-IR (KBr, cm⁻¹): (p(AMPS-Na⁺-co-VIm)-BB): 3442 (br, s), 3246 (shoulder), 3136 (w), 3082 (w), 2916 (m), 2851 (w), 1657 (s), 1565 (m), 1555 (m), 1500 (w), 1449 (m), 1365 (w), 1226 (w), 1164 (s), 1107 (w), 1086 (m), 1029 (w), 951 (w), 910 (w), 835 (m), 754 (m), 655 (m), 618 (w), 529 (w).



Scheme 1 Schematic representation of p(AMPS- H^+ -co-VIm)-Ag, p(AMPS- Na^+ -co-VIm)-Ag and nano-composites and modification of p(AMPS- Na^+ -co-VIm) hydrogel with 1,4-dibromobutane

2.6 Determination of the Amount of Silver Within Hydrogel Matrix

The amount of metal ion within the hydrogel matrix was determined by using Atomic Absorption Spectroscopy using metal ion solution obtained by treating 25 mg p(AMPS- H^+ -co-VIm)-Ag and p(AMPS- Na^+ -co-VIm)-Ag with 4 mL HNO_3 (conc.) three times for 18 h to dissolve Ag ions.

2.7 General Oxidation Procedure

A mixture of silver composite in H_2O (3.0 mL) was placed into a two-necked flask equipped with a magnetic stirrer. The flask was evacuated and refilled with pure oxygen (balloon filled). Then the benzyl alcohol (1.0 mmol) and K_2CO_3 (1.5 mmol) were added into the solution with a syringe. Then the solution was introduced to continue the reaction in the stable temperature. The resulting mixture was vigorously

stirred at 60 °C under O₂ atmosphere for 6 h. The oxidation products were identified by comparing the retention times with the literature data. To test the reusability of the composites, after every usage, the catalyst was separated from reaction mixture by filtration, washed with ethanol and reused in the same reaction conditions again.

2.8 Adsorption Study

The potential of prepared bare and composite hydrogels to be used as adsorbent was investigated by carrying out the adsorption studies of Benzyl alcohol, BA, from water. The effect of various factors on adsorption of BA, such as different dose of hydrogel on adsorption of BA was explored systematically to get optimized adsorption circumstances. In the common adsorption research, 0.1 g of hydrogel was added in 40 mL BA solutions (100 mg L⁻¹) for 6 h. The adsorption process was performed at room temperature with constant magnetic stirring. 1 mL sample was removed from the reaction mixture at different times. Then, these samples were diluted with distilled water about 3 times. This dilution was related with initial concentration. After 6 h, the hydrogel was removed and filtered. The concentration of the BA remained in the dye solutions was determined by using UV/Vis spectrophotometer at 259 nm as λ_{max} of BA. Adsorption efficiency or percentage removal was calculated by applying the following equation: [14, 15]

$$\text{Removal \%} = \frac{(C_0 - C_e)}{C_0} \times 100, \quad (1)$$

where C₀ and C_e are the respective initial and equilibrium concentration of benzyl alcohol solutions (mg/L) [13]. The effect of adsorbent dose on the adsorption capacity was considered by different amount of hydrogel from 0.05 to 0.2 g under the equal experimental circumstances and the percentage removal was explored by applying Eq. (1).

Selected FT-IR (KBr, cm⁻¹): (p(AMPS-Na⁺-co-VIm)): 3450 (br, s), 3107 (shoulder), 2989 (w), 2933 (w), 1662 (vs), 1547 (s), 1393 (m), 1372 (w), 1302 (w), 1225 (m), 1193 (w), 1161 (w), 1119 (m), 1087 (w), 1051 (s), 915 (w), 862 (w), 819 (w), 766 (w), 670 (w), 627 (m), 531 (w).

Selected FT-IR (KBr, cm⁻¹): (p(AMPS-Na⁺-co-VIm)/BA): 3424 (br), 3110 (shoulder), 2925 (w), 2851 (w), 1668 (vs), 1494 (s), 1454 (m), 1416 (m), 1287 (m), 1228 (s), 1087 (s), 1015 (vs), 918 (s), 825 (m), 748 (m), 662 (s), 633 (w).

3 Results and Discussion

3.1 Synthesis and Characterization

The characterization of porous p(AMPS-H⁺-co-VIm) and p(AMPS-Na⁺-co-VIm) hydrogels and their metal composites were carried out with various characterization techniques, such as SEM images, FT-IR spectroscopy, HRXPS, TEM images, EDX and AA spectroscopy.

The structure of p(AMPS-H⁺-co-VIm) and p(AMPS-Na⁺-co-VIm) hydrogels, were determined using a Scanning Electron Microscope (SEM, JEOL 2010) on thin sections of freeze dried p(AMPS-H⁺-co-VIm) and p(AMPS-Na⁺-co-VIm) hydrogels, as shown in Fig. 1a, b, respectively. The SEM image of p(AMPS-Na⁺-co-VIm), Fig. 1c, d, indicates the formation of homogeneous and highly porous material in comparison with p(AMPS-H⁺-co-VIm) hydrogel, Fig. 1a, b.

To determine the swelling behavior of p(AMPS-H⁺-co-VIm) and p(AMPS-Na⁺-co-VIm) hydrogels, distillation water was chosen as the swelling media. The swelling ratios were estimated using the following equation:

$$\text{Swelling ratio (\%)} = \left[\frac{(W_s - W_d)}{W_d} \right] \times 100,$$

where W_s is the weight of swollen hydrogel and W_d is the weight of the dried hydrogel at time zero.

The results indicated that in an aqueous environment (water), the p(AMPS-H⁺-co-VIm) hydrogel had a swelling value of 340%. The swelling value of the p(AMPS-Na⁺-co-VIm) hydrogel was 1200%. It can be declared that the osmotic pressure of the p(AMPS-Na⁺-co-VIm) is boosted owing to the presence of the detached sodium sulfonate groups. On the one hand, the polymer coils are enlarged because the negatively charged sulfonate groups keep each other away. On the other hand, the positively charged sodium salt prevents the polymer coils from an excessive extension [16]. When the polymer is surrounded by water, it penetrates the pores of the polymer network. The driving force for swelling is the difference between the osmotic pressure inside and outside the polymer membrane. As the results revealed, the swelling value of the p(AMPS-Na⁺-co-VIm) hydrogel exceeded that of the p(AMPS-H⁺-co-VIm) hydrogel. This finding can be ascribed to three issues. First, in the p(AMPS-Na⁺-co-VIm) hydrogel, the ionic osmotic pressure is greater due to the existence of salt (AMPS-Na⁺). Second, the bigger Na⁺ ions are surrounded by the hydrogel, which creates copolymer chains between crosslinking points and allows the structure to extend as much as possible. Third, AMPS-H⁺ has greater acidity, which probably leads to the chain scission of the copolymer [17, 18].

The representative FT-IR spectra of p(AMPS-Na⁺-co-VIm) and p(AMPS-H⁺-co-VIm) are shown in Fig. 2. Both

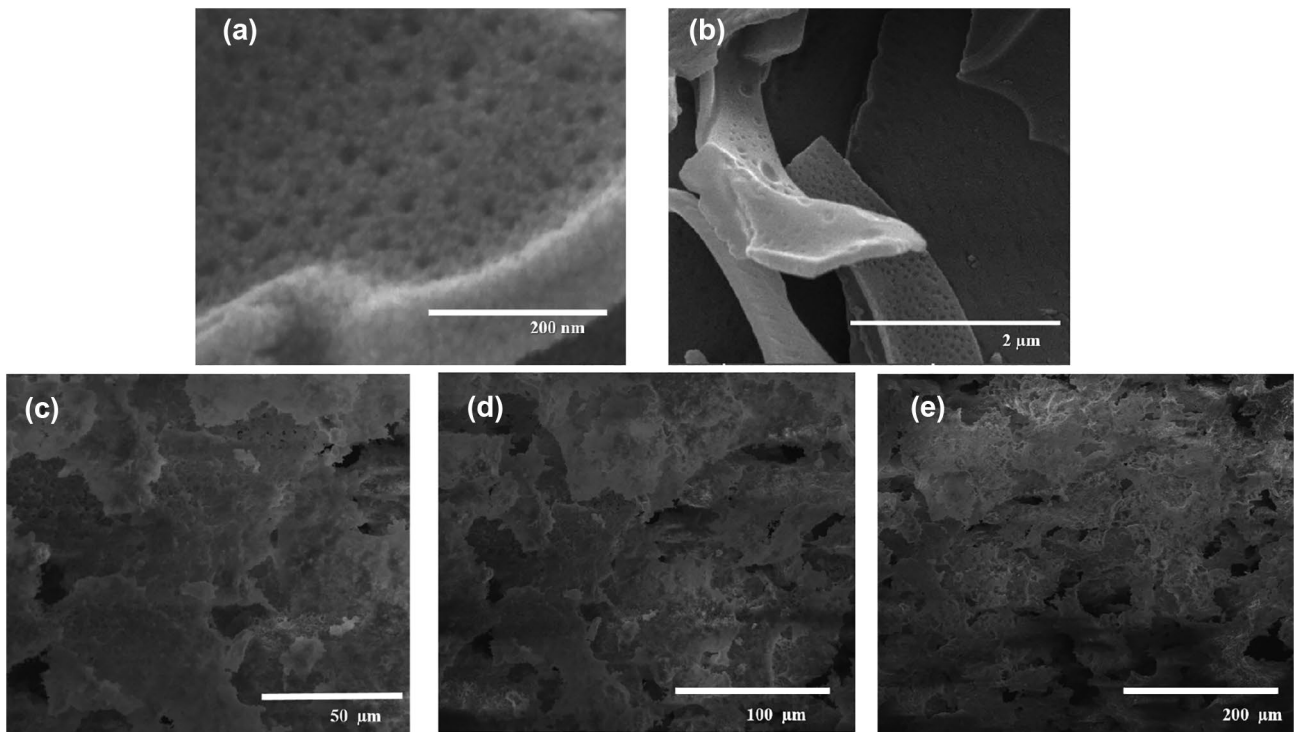


Fig. 1 SEM image of **a, b** p(AMPS-H⁺-co-VIm) hydrogels, **c, d, e** p(AMPS-Na⁺-co-VIm) hydrogels

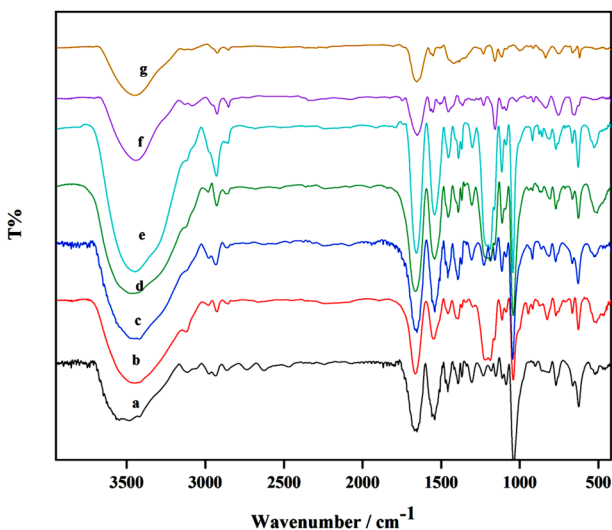


Fig. 2 FT-IR spectra of (a) p(AMPS-H⁺-co-VIm), (b) p(AMPS-H⁺-co-VIm)-Ag, (c) p(AMPS-Na⁺-co-VIm), (d) p(AMPS-Na⁺-co-VIm)-Ag, (e) recycled p(AMPS-Na⁺-co-VIm)-Ag, (f) p(AMPS-Na⁺-co-VIm)-BB, (g) p(AMPS-Na⁺-co-VIm)-BB-Ag

spectra showed absorption peak at around 3000–3500 cm⁻¹ stretching frequency of the O–H and N–H groups [19], and bands at 2989 and 2933 cm⁻¹ correspond to aliphatic –CH stretching. A sharp peak of C=O stretching of the amide I at around 1664 cm⁻¹ (Fig. 2a) and 1663 cm⁻¹ (Fig. 2c) and

a strong peak of the N–H bending of amide II at 1547 cm⁻¹ (Fig. 2a) and 1542 cm⁻¹ (Fig. 2c). The relative weak peaks at 1460 cm⁻¹ (Fig. 2a) and 1453 cm⁻¹ (Fig. 2c) along with those at 1664 cm⁻¹ and 1663 cm⁻¹ are the symmetrical and asymmetrical C(=O)₂ stretching. Importantly, the sharp and strong peaks of the S=O stretching of AMPS-Na⁺ and AMPS-H⁺ at 1051 cm⁻¹ (Fig. 2a) [20] and 1037 cm⁻¹ (Fig. 2c) [21] were observed, respectively. Another two strong and sharp peaks at 1182 cm⁻¹ (Fig. 2a) and 1186 cm⁻¹ (Fig. 2c) arose from the C–C(=O)–O stretching. A relatively board and strong peak at 3456 cm⁻¹ in Fig. 2a is for the NH or the OH stretching of p(AMPS-Na⁺-co-VIm) where that for p(AMPS-H⁺-co-VIm) (Fig. 2c) becomes very board at 3415 cm⁻¹ because the OH group in the free acid superimposed the NH stretching of acrylamide moiety. And finally, the chemical changes in the structure of p(AMPS-Na⁺-co-VIm)-Ag and p(AMPS-H⁺-co-VIm)-Ag composites were confirmed via FT-IR spectroscopy. After loading of Ag ions and reduction to Ag nano-particles, the small shifts in FT-IR spectra of compounds are related to interactions between Ag and hydrogel matrix, as shown in Fig. 2 and b, d.

A schematic representation of metal loading and in situ reduction process for the formation of metal nanoparticles inside hydrogel networks is demonstrated in Scheme 1. To investigate the nanostructure of the sample, TEM and EDS measurement was carried out. The TEM images of metal nanoparticles-containing p(AMPS-Na⁺-co-VIm) and

p(AMPS-H⁺-*co*-VIm) hydrogels are given in Figs. 3 and 4. As can be seen, metal nanoparticles with a uniform spherical shape, about < 20 nm are distributed within p(AMPS-Na⁺-*co*-VIm) and p(AMPS-H⁺-*co*-VIm)-Ag hydrogel matrices. In addition, according to the EDS results, Ag prevent loading in p(AMPS-Na⁺-*co*-VIm)-Ag is more than p(AMPS-H⁺-*co*-VIm), ~ 30% and ~ 9%, respectively. These results have been confirmed by AA results, previously (see Tables 1 and 2).

The HRXPS analysis is conducted to examine how metal nanoparticles and hydrogel functional groups interact with each other. The exact binding energy of an electron is determined by three factors: the level of photoemission, the formal oxidation state of the atom, and the characteristics of the environment. To analyze these factors, the HRXPS spectra would be of great help since this technique has the capability to differentiate various oxidation states and chemical environments. In elevated positive oxidation states, an additional columbic interaction takes place between the photoemitted electron and the ion core, which generates a greater amount of binding energy.

The spectrum of the p(AMPS-Na⁺-Ag) nanocomposite (Fig. 5a) confirmed the presence of C, O, S, N, and Ag in the hydrogel matrix. This result revealed that the organic moieties and Ag-NPs were incorporated into the structure of the hydrogel. The results also exhibited the deconvolution of C1s into three peaks (Fig. 5c): (1) a peak pertaining to the C–N and C–S bonds at 285.08 eV, (2) a peak related to the C–C or C–H bonds at 283.96 eV, and (3) a peak associated with the H₂N–C=O bond in the AMPS-Na⁺ and MBA at 287.44 eV [22, 23]. Illustrating the N1s spectra of the p(AMPS-Na⁺-*co*-VIm)-Ag nanocomposite, Fig. 5d displays two peaks: (1) a peak generated by the interaction of C–N, CO–NH₂ in AMPS-Na⁺ and Ag nanoparticles at 399.76 eV, and (2) a peak formed by the interaction of the imidazole ring functional groups in the hydrogel and Ag nanoparticles at 400.30 eV. It seems that the electrons in the Ag nanoparticles moved toward the functional groups, which brought about a boost in the electron density of the nitrogen atoms and a reduction in their binding energy. Previous studies have also obtained the same results [24]. Furthermore, the nitrogen and metal atoms were interacted, which elevated the charge density of the Nitrogen atoms and eventually declined the N1s BE value. The presence of a covalent bond between the metal atoms and the functional group of the polymer (i.e., nitrogen atoms) was verified via the XPS analysis. The S2p spectra of the p(AMPS-Na⁺-*co*-VIm)-Ag nanocomposite, as shown in Fig. 5f, indicate that the S2p core-level spectrum at the BE value of approximately 163.21, 168.45 eV is similar to the spectrum of the covalently bonded sulfonic acid group (–SO₃[–]) in the hydrogel [25, 26]. Figure 5e and d show the high-resolution O 1s spectra obtained from the p(AMPS-Na⁺-*co*-VIm)-Ag nanocomposite. Two peaks at 528.88 and 531.81 eV related to the metal oxide and adsorbed H₂O, respectively. Figure 5b depicts the 3d spectrum of Ag

nanoparticles. The wide scan spectrum shows that the Ag 3d doublet peaks were formed, which confirms the generation of Ag nanoparticles in the p(AMPS-Na⁺-*co*-VIm)-Ag nanocomposite. Two peaks appeared: a peak pertaining to the Ag 3d_{3/2} transition at 374.87 eV and a peak corresponding to the Ag 3d_{5/2} transition at 368.86 eV. The development of these peaks can be ascribed to either the formation of Ag–N bonds or the interaction of the metal atoms and the functional groups in the *co*-polymer. The spin energy between the two peaks was calculated as 6.01 eV, it can be stated that metallic Ag nanoparticles are formed and the Ag nanoparticles have a zero oxidation state [27–29]. In comparison with the standard binding energies of pure Ag (368.0 and 374.0 eV), the obtained binding energies of the Ag 3d peaks (Ag 3d_{3/2} and Ag 3d_{5/2}) were higher because electrons in metallic silver were transferred to the functional groups of the hydrogel. Hence, it can be declared that there was an interaction between the Ag nanoparticles and the functional groups of the hydrogel, and the Ag nanoparticles were successfully generated in the hydrogel network.

The representation of the modification mechanism of porous p(AMPS-Na⁺-*co*-VIm) hydrogels is given in Scheme 1. After quaternization, the chemical changes in the structure of p(AMPS-Na⁺-*co*-VIm) hydrogels were confirmed via FT-IR spectroscopy by recording the FT-IR spectra of Q-p(AMPS-Na⁺-*co*-VIm) and Q-p(AMPS-Na⁺-*co*-VIm)-Ag, Fig. 2f and g. As seen in Fig. 2f, after quaternization, –N–C and –C–H bending coming from newly quaternized ⁺NR (R: C₂H₄) groups were observed at 1560 cm^{–1} and 1360 cm^{–1} and intensities of these peaks increased according to the length of alkyl chain, respectively. Also, the new absorption band that occurred at 1160 cm^{–1} upon quaternization corresponded to C–N stretching. This new peak confirmed the interaction between the methyl group and the N atom in the ring [30]. The intensity of this stretching increased with quaternization. The –C=N and –C=C bands in aromatic rings were observed for each modified polymer.

The amount of metal ion within the hydrogel matrix was determined by using Atomic Absorption Spectroscopy after HCl:HNO₃ treatment; silver was 0.198 mmol g^{–1} hydrogel and for p(AMPS-Na⁺-*co*-VIm)-Ag/H₂O and 0.042 mmol g^{–1} hydrogel for p(AMPS-H⁺-*co*-VIm)-Ag/H₂O and 0.283 mmol g^{–1} hydrogel for p(AMPS-Na⁺-*co*-VIm)-BB-Ag composites, respectively.

3.2 Catalytic Activity of p(AMPS-Na⁺-*co*-VIm)-Ag⁰ and p(AMPS-H⁺-*co*-VIm)-Ag⁰

3.2.1 Oxidation of Alcohols by p(AMPS-Na⁺-*co*-VIm)-Ag⁰ and O₂/TBHP as Oxidant

One of the most critical reactions in organic synthesis is the selective oxidation of alcohols. In this reaction, O₂ is usually

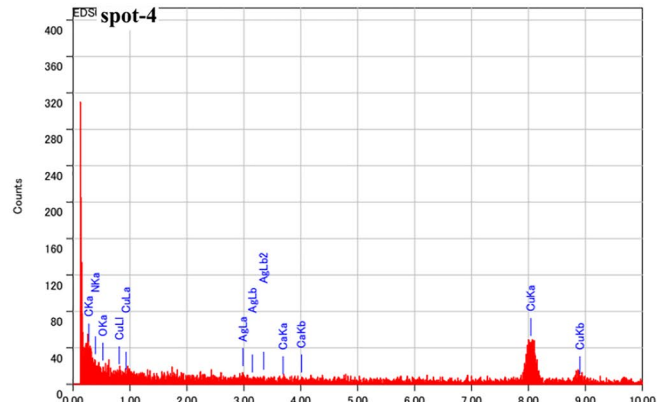
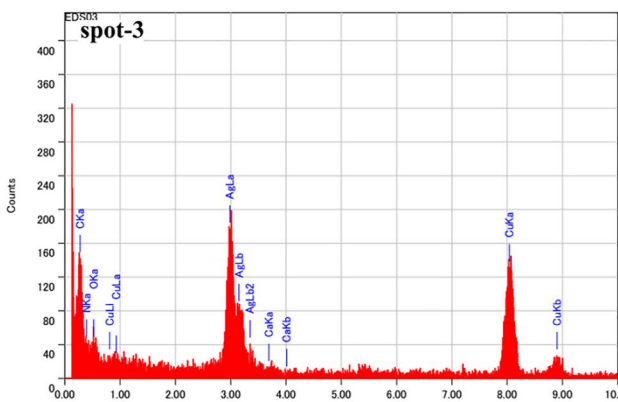
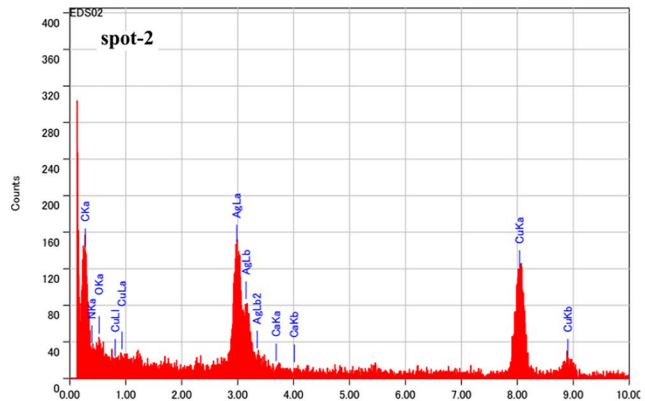
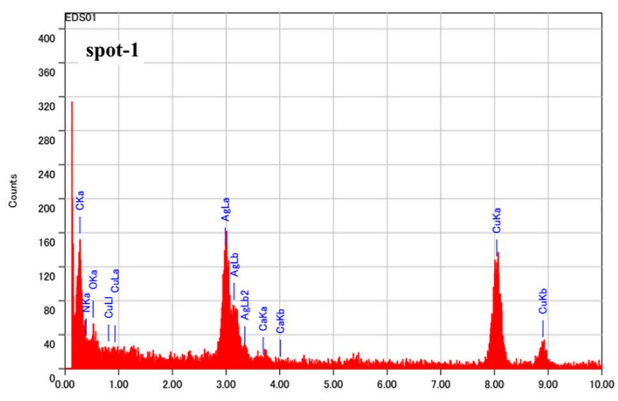
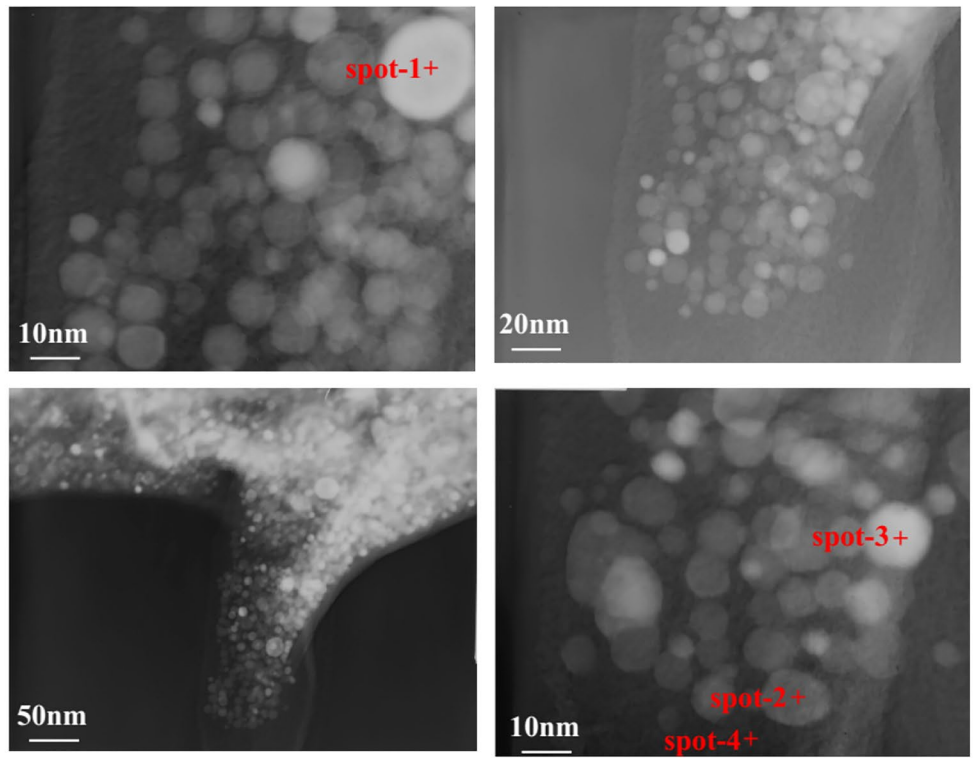


Fig. 3 TEM images of metal nanoparticles from p(AMPS- Na^+ -co-VIm)-Ag and EDX spectra of p(AMPS- Na^+ -co-VIm)-Ag

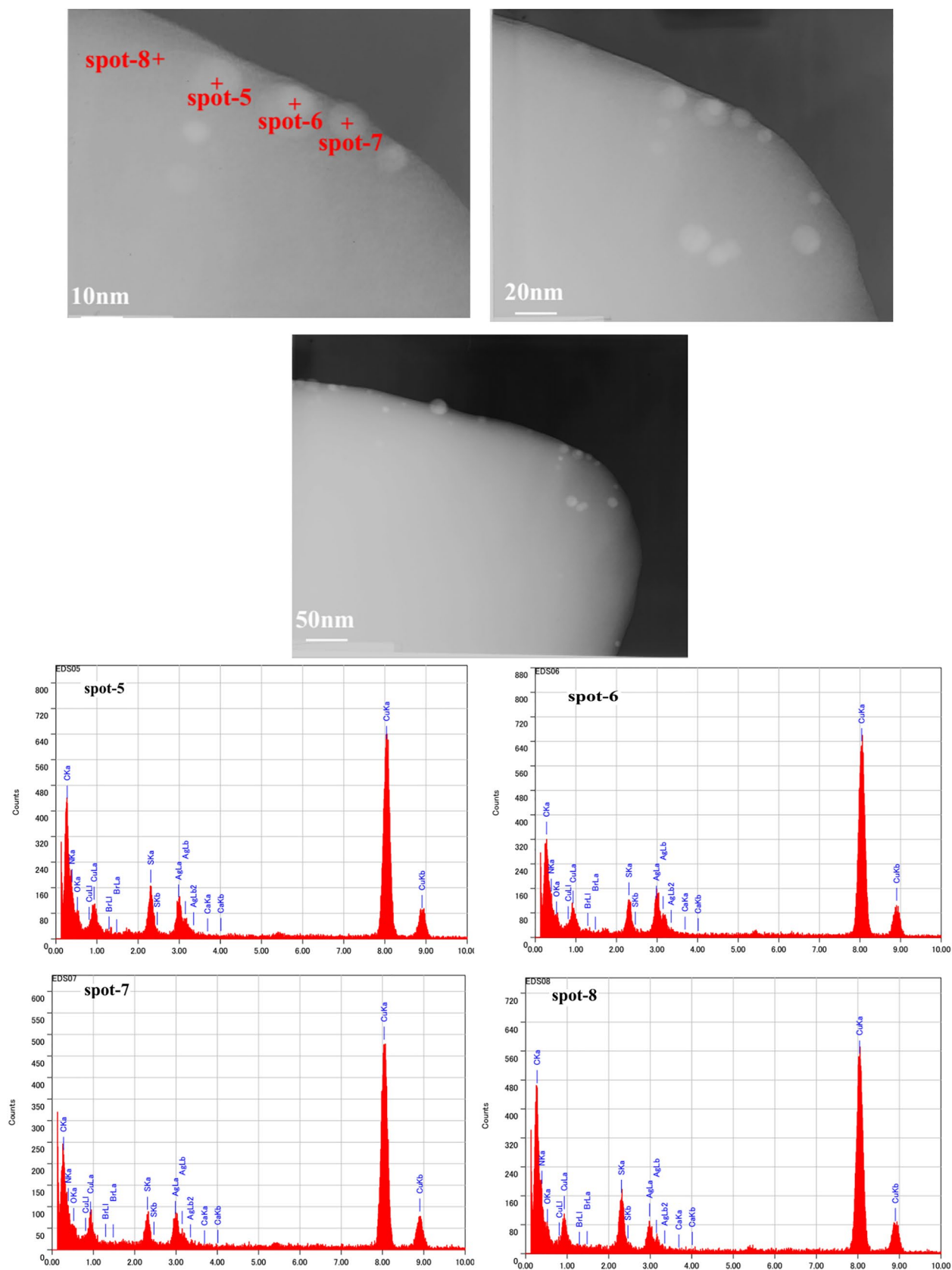


Fig. 4 TEM images of metal nanoparticles from p(AMPS- H^+ -co-VIm)-Ag and EDS spectra of p(AMPS- H^+ -co-VIm)-Ag

Table 1 EDS results of p(AMPS-Na⁺-co-VIm)-Ag at 1, 2, 3, 4 spots

Spot number	Element	Mass %	Count	Atomic %
1	Ag	33.98	1276.69	8.18
	C	32.34	1054.40	69.92
	N	4.31	236.10	7.98
	S	–	–	–
	O	1.47	113.20	2.39
2	Ag	33.15	1126.51	8.06
	C	33.97	1001.89	74.22
	N	1.82	90.03	3.40
	S	–	–	–
	O	1.13	78.92	1.86
3	Ag	33.37	1577.46	9.36
	C	30.66	1123.44	68.98
	N	3.73	229.69	7.19
	S	–	–	–
	O	1.91	165.17	3.23
4	Ag	1.87	15.14	0.36
	C	40.34	284.03	69.98
	N	9.14	108.16	13.59
	S	–	–	–
	O	–	–	–

Table 2 EDS results of p(AMPS-H⁺-co-VIm)-Ag at 5, 6, 7, 8 spots

Spot number	Element	Mass %	Count	Atomic %
5	Ag	9.62	1029.86	2.27
	C	27.96	2596.86	59.32
	N	7.35	1148.91	13.38
	S	3.42	1196.05	2.72
	O	1.35	296.75	2.16
6	Ag	12.90	1231.76	3.66
	C	21.99	1822.69	55.99
	N	3.68	512.32	8.02
	S	2.99	934.58	2.85
	O	0.95	185.87	1.82
7	Ag	9.48	629.97	2.68
	C	21.87	1260.86	55.52
	N	3.71	359.75	8.08
	S	2.97	645.42	2.83
	O	0.81	110.66	1.55
8	Ag	6.4	622.95	1.40
	C	32.40	2737.14	63.46
	N	7.30	988.76	11.81
	S	4.04	1285.63	2.96
	O	1.65	329.77	2.43

utilized as a terminal oxidant. In current study, the catalytic behavior of p(AMPS-Na⁺-co-VIm)-Ag⁰ in the process of the aerobic oxidation of alcohols is assessed. Table 3 reports some of the achieved results.

To maximize the transformation, initially, optimal reaction conditions should be identified and provided. To this end, alcohol conversion was measured with different amounts of the catalyst. Moreover, according to the literature, another influential factor in alcohol conversion is temperature. Therefore, the oxidation reaction of alcohol was also assessed at various temperatures. The results showed that with a boost in temperature, the rate of alcohol conversion was raised. When the temperature was increased (from 25 to 60 °C), the conversion increased correspondingly (from 0% to 35.5%). So, in continuous the oxidation reaction of the benzyl alcohol as the model substrate was done in water at 60 °C. The blank experiments without Ag loading exhibits a negligible benzyl alcohol conversion (< 7% at 60 °C and 6 h reaction time). No benzaldehyde/benzoic acid was obtained without the use of a catalyst. However, in the presence of the Ag catalyst, benzyl alcohol conversion increases [31]. To be more precise, benzaldehyde with an isolated yield of 35.5% was obtained after six hours by using 0.0125 g of the catalyst. When 0.025 g of the catalyst was added, benzaldehyde with an isolated yield of 65.4% was

achieved after six hours, (Table 3, entries 1–2). Nonetheless, with greater amounts of catalyst (from 25 to 50 mg), the conversion rate lessened (from 65.4% to 60%). This decline can be attributed to a reduction in the concentration of the substrate transmitted by catalyst, which decreased the collision of the silver nano-catalyst, the oxidant (O₂), and the substrate [30]. These findings corroborate that in order to create the most effective condition for alcohol conversion, the optimal amount of catalyst is 25 mg (0.005 mmol Ag).

To assess the generalizability of the results, other types of alcohols were oxidized with the different substituent such as 4-MeO, 4-NO₂ and 4-Cl groups (Table 3, entries 3–5). The substitution effect on aromatic substrates was studied. The results demonstrated that when electron-donating substituents were used, such as –OMe at the *para*- position of benzyl alcohol, the alcohol conversion rate was promoted. On the contrary, the use of the withdrawing group, such as NO₂ and Cl, led to a drop in this rate [32]. This trend is in accord with *Hammett* plot results and suggesting that the formation of the transition state with a carbocationic character on the benzylic carbon during the discharge of hydrogen in the rate-determining step is involved in the oxidation pathway over the present catalysts [33].

Ultimately, to confirm the hydrogel matrix species effects on catalytic activity of composites, catalytic activity of p(AMPS-Na⁺)-Ag, and p(VIm)-Ag were also investigated under optimized reaction conditions in the presence of same molar amount of Ag, as shown in Table 3, entries 5–6.

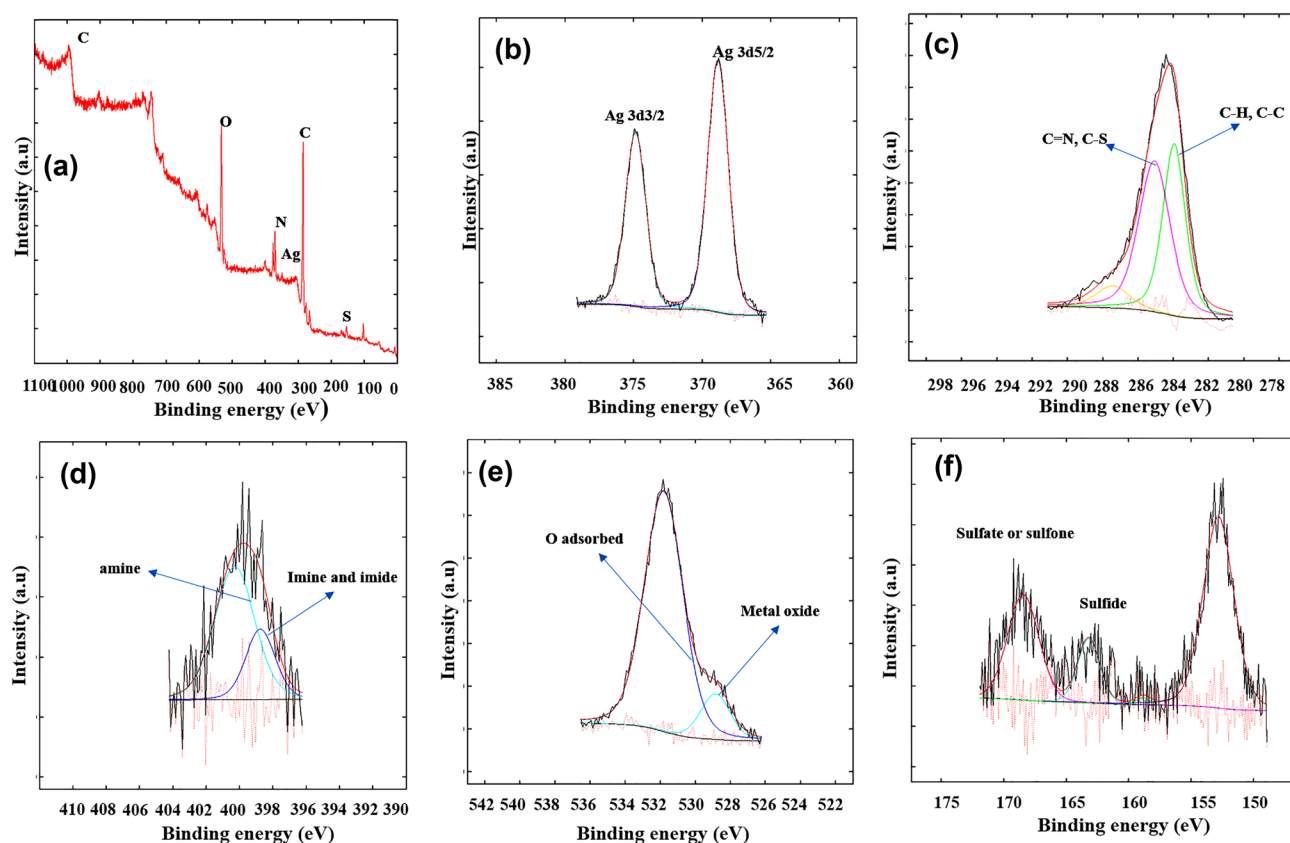


Fig. 5 HRXPS spectra of **a** survey of p(AMPS-Na⁺-co-VIm)-Ag, **b** Ag 3d, **c** C 1 s, **d** N 1 s, **e** O 1 s, **f** S 2p of p(AMPS-Na⁺-co-VIm)-Ag

According to the results, p(AMPS-Na⁺)-Ag, and p(VIm)-Ag composites showed less activity than p(AMPS-Na⁺-co-VIm)-Ag nanocomposites. It was concluded from these results that it may be due to the synergistic effect of VIm aromatic ring and amid group of AMPS-Na⁺, in adsorption and effective interaction between catalyst, oxidant and substrate which dramatically altered the catalytic performance of the composite.

The catalytic oxidation of benzyl alcohol was also carried in the presence of TBHP by using p(AMPS-Na⁺-co-VIm)-Ag as catalyst. It is required to detect the optimized amount of the catalyst precursor to achieve the best result. Hence, three amounts of the catalyst (0.0125, 0.025 and 0.05 g equal to 0.0025 mmol, 0.005 mmol and 0.01 mmol Ag, respectively) were considered in the experiment while the amount of benzyl alcohol (1 mmol) and other reaction parameters were constant (TBHP 1 mmol and temperature 60 °C).

By increasing the amount of catalyst from 0.0125 to 0.025 g, the conversion increased from 43.5% to 78%. The benzyl alcohol conversion is low at 0.0125 g catalyst, which is due to the presence of fewer catalytic sites. It is generally believed that by increasing the catalyst amount, better chances are there for the reactants to gain more active sites. But, the selectivity for benzaldehyde decreases unavoidably

with increasing the catalyst amount. According to the literature, by using higher amounts of catalysts, it is more probable that a greater number of active sites are accessible to reactants. On the other hand, greater amounts of catalysts bring about a decline in the selectivity for aldehyde since a higher amount of aldehyde is oxidized to benzoic acid [34].

Furthermore, the conversion rate with 0.05 g of the catalyst was approximately the same as that with 0.025 g of the catalyst. These findings reveal that to obtain the most efficient conversion and selectivity rate, the optimal amount of catalysts is 0.025 g. It was also observed that there was a drop in benzyl aldehyde selectivity. It seems that with the increment of catalytic reactions, the generated aldehyde is constantly oxidized, which induces the formation of benzoic acid. These processes eventually weaken the selectivity percent [35–37] (Table 3, entries 1–3).

In addition, the reaction was carried out at different temperatures. The benzyl alcohol conversion was lower at 25 °C, which is due to the thermal effect on the kinetically controlled reaction. When the temperature was increased (from 25 to 60 °C), the conversion increased correspondingly (from 10% to 78%). The results also revealed that the higher the temperature, the greater the conversion rate. However, there was a reduction in aldehyde selectivity [34]. When the

Table 3 Catalytic activity of p(AMPS- Na^+ -*co*-VIm)-Ag on the oxidation of benzyl alcohol

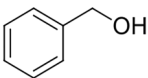
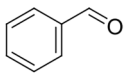
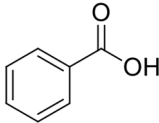
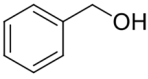
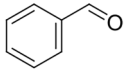
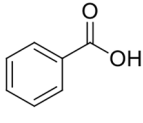
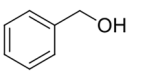
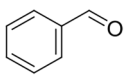
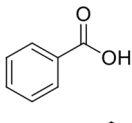
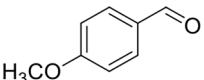
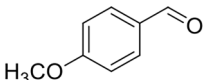
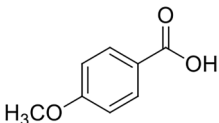
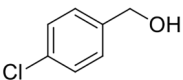
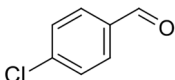
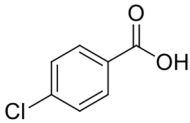
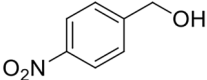
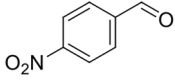
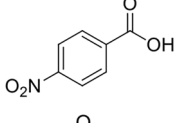
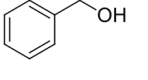
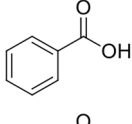
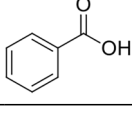
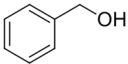
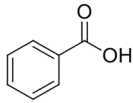
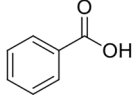
Entry	Substrate	Conversion ^a (%) O ₂ /TBHP	Product	Selectivity (%) O ₂ /TBHP
1 ^b		35.5/43		> 99/73.5
				-/26.5
2 ^c		65.4/78		92/64
				8/36
3 ^d		60/82		85/60
				15/40
3 ^e		78/87		88/50
				12/50
4 ^e		32/48		94/56
				6/44
5 ^e		24/32		> 99/59
				-/41
5 ^e		12/18		> 99/> 99
				-/-

Table 3 (continued)

Entry	Substrate	Conversion ^a (%) O ₂ /TBHP	Product	Selectivity (%) O ₂ /TBHP
6 ^f		20/28	 	> 99/> 99 -/-

Catalyst (p(AMPS-Na⁺-co-VIm)-Ag), substrate (1.0 mmol), H₂O (5 mL) as solvent, Na₂CO₃ 1.2 mmol, temperature 60 °C, Time = 6 h under O₂ atmosphere

^aConversions are based on the starting substrate

^bCatalyst (0.0125 g)

^cCatalyst (0.025 g)

^dCatalyst (0.005 g)

^eCatalyst (p(AMPS-Na⁺)-Ag (0.005 mmol Ag)

^fCatalyst {(p(VIm)-Ag 0.005 mmol Ag}

temperature was raised from 60 to 80 °C, the selectivity to benzaldehyde decreases, due to the rapid decomposition of TBHP combined with further oxidation of benzaldehyde to benzoic acid at the high temperature. Nevertheless, at high temperatures, TBHP decomposed quickly and more aldehyde was oxidized to acid. Therefore, there was a decline in aldehyde selectivity. Hence, it is required to determine the optimal temperature to have an effective trade-off between aldehyde selectivity and alcohol conversion. In this study, the optimal temperature was 60 °C. It can be stated that as reaction temperature increases, the miscibility of a catalyst with reactants is boosted. But, at temperatures above 60 °C, TBHP is decomposed, which leads to inadequate alcohol oxidation and reaction yields [38]. Therefore, 60 °C was considered as the ideal reaction temperature by considering the balance between benzaldehyde selectivity and benzyl alcohol conversion.

Finally, three different amounts of oxidant (TBHP) viz. 0.5, 1 and 1.5 mmol were tested. The amount of TBHP used in this reaction is one of the most influential factors in alcohol oxidation reactions. Low conversion of benzyl alcohol is observed, when the ratio of the substrate to the oxidant was the same as or less than the stoichiometric ratio. The benzyl conversion was augmented with an increase in the ratio of the substrate to the oxidant. It clearly indicates that the increase in the TBHP amount considerably increases the conversion of benzyl alcohol [39]. However, higher amount of TBHP leads to over oxidation of benzaldehyde to benzoic acid. Hence, excessive volumes of TBHP adversely impact aldehyde selectivity. Based on the above results, the optimal molar ratio of TBHP/BzOH is (1 mmol). With the aim of examining the catalytic potential of p(AMPS-Na⁺-co-VIm)-Ag towards other alcohols, various aromatic

electron-donating and electron-withdrawing alcohols were examined. The obtained results are listed in Table 3.

It was also found that being a greater oxidizing agent, TBHP promoted the conversation rate more than O₂ [40]. One possible reason why the activity of the catalyst is reduced using O₂ is that in gas-liquid-solid catalytic reactions, benzyl oxidation is restricted because of the mass transfer resistance [35, 41].

Moreover, TBHP was an amphiphilic oxidant and the substrate was hydrophobic, the hydrophobic tail of TBHP (*t*-But) interacted with the substrate. The catalyst was hydrophilic, hence the hydrophilic head of TBHP (OOH) interacted with catalyst. The hydrophilic VIm and AMPS moieties in the framework, had a considerable impact on enhancing catalytic activities by enhancing the accessibility of TBHP, and accelerate transferring substrate to the active site of catalyst [42]. But in the presence of O₂ as an oxidant, diffusion of substrate happens slowly. Consequently, it can be postulated that compared to O₂, TBHP is a more promising option for alcohol oxidation.

Moreover, as TBHP was an amphiphilic oxidant and the substrate was hydrophobic, the hydrophobic tail of TBHP (*t*-But) interacted with the substrate. The catalyst was also hydrophobic, hence, the hydrophobic head of TBHP (OOH) also interacted with this catalyst. The hydrophilic VIm and AMPA moieties had a considerable impact on enhancing catalytic activities. Therefore, it is possible to obtain optimal catalytic reactions by increasing accessibility to TBHP and raising the pace of substrate transfer to the active sites of the catalyst. When O₂ was used as an oxidant, the substrate dispersed gradually, and eventually, no favorable results were obtained. Consequently, it can be postulated

that compared to O₂, TBHP is a more promising option for alcohol oxidation.

In this study, the catalytic behavior of the p(AMPS-Na⁺-*co*-VIm)-Ag hydrogel was compared with that of the p(AMPS-H⁺-*co*-VIm)-Ag hydrogel. The same amount of Ag⁰, 0.005 mmol, was included in these reactions. It was observed that the catalytic activity of the p(AMPS-Na⁺-*co*-VIm)-Ag hydrogel exceeded that of the p(AMPS-H⁺-*co*-VIm)-Ag hydrogel. The higher oxidation rate in the presence of p(AMPS-Na⁺-*co*-VIm)-Ag can be attributed to its favorable porous structure and size. To be more precise, in p(AMPS-Na⁺-*co*-VIm)-Ag, there is greater accessibility to Ag nanoparticles, as catalytic active sites, because of the low penetration of the substrate and the solvent into the small pores of the p(AMPS-H⁺-*co*-VIm) hydrogel. Similarly, the p(AMPS-H⁺-*co*-VIm)-Ag catalyst displayed greater catalytic reactions with TBHP than with O₂ (see Table 4).

To compare the catalytic activity of p(1-VIm) hydrogels modified with butyl chain, we used same amount of Ag⁰ in the catalytic reactions. The oxidation reaction was carried out with 1,4-BB modified p(AMPS-Na⁺-*co*-VIm)-Ag metal composites containing 0.005 mmol silver particles under the reaction conditions as given in material and methods section, as shown in Table 5. As quaternized composites have great hydrophobicity, high alcohol conversion rates were gained with both oxidants (TBHP, O₂). These conversion rates were higher than those of their un-quaternized counterparts. Another explanation for the favorable catalytic activity of the modified catalysts is associated with their hydrophobic features. In other words, the inclusion of alkyl chains improved the hydrophobicity of the catalyst, which augmented the interaction of the modified catalyst with the hydrophobic substrate. Hence, the amphiphilicity of the composite increased and the catalyst could easily penetrate the hydrogel. These processes enhanced the interaction between the substrate and the modified catalyst and raised access to the catalytic active sites, which eventually increased the conversion rate [43]. The miscibility/high solubility between 1,4-BB-p(AMPS-Na⁺-*co*-VIm)-Ag, substrate and solvent played an important role for oxidation efficiency. An in the same way 1,4-BB-p(AMPS-Na⁺-*co*-VIm)-Ag showed better catalytic activity in the presence of TBHP than O₂ as an oxidant.

Among other advantages of this catalyst are simple preparation and purification processes, insolubility, reusability, and recyclability. This catalyst, as a porous complex, can be utilized as biphasic catalysts for certain reactions, such as alcohol oxidation. In this solid-liquid biphasic systems, it is feasible to recover the catalyst and reuse it without any change in the catalyst structure. In the current study, the reusability and stability of p(AMPS-Na⁺-*co*-VIm)-Ag were measured for 4 runs. After each run, ethanol and water were utilized to wash the filtrated solid catalyst. Afterward, the

catalyst was dried and used in the next run. The results demonstrated that the catalyst had the same catalytic behavior in all four runs, 78%, 79%, 77%, 75%, respectively, which verifies its high stability. The reaction mixture separated from the catalyst was studied via atomic absorption spectroscopy. The results revealed the absence of free silver ions in the mixture, which proves that no catalyst leaching occurs. The p(AMPS-Na⁺-*co*-VIm)-Ag hydrogel separated from the solution after four runs were analyzed through the FT-IR spectrum, and the achieved results were similar to the FT-IR spectrum of the fresh p(AMPS-Na⁺-*co*-VIm)-Ag catalyst. These findings confirm that the catalyst has an excellent robust and stable structure and it is feasible to recycle it efficiently, Fig. 2e.

A hypothesis of the possible mechanism of catalytic oxidation of alcohols by silver nanocomposites was presented in Scheme 2.

Deprotonation of alcohol was promoted by Na₂CO₃ to form alkoxide on the Ag surfaces. Ag catalyzes the β-hydride elimination to produce corresponding aldehyde along with the formation of O₂ and H₂O. As shown in Scheme 3a, alcohol converted to aldehyde then H₂O and O₂ are released. Aldehyde is the first product of this process whereas carboxylic acids can generally be obtained in two steps in an aqueous medium, via the in situ generation of geminal diol through hydration of aldehyde followed by oxidation into the corresponding carboxylic acid (Scheme 2a).

The proposed mechanism for oxidation of alcohols in the presence of TBHP is as shown in Scheme 2b. Since the oxidation of alcohols is an oxidation-reduction reaction, first, the Ag nanoparticles are oxidized to silver oxide species with *tert*-BuOOH. Then, the alcohol is attached to the Ag oxide species via an addition step to produce the intermediate I which in turn releases H₂O and give the intermediate II. This intermediate is converted to final product and releases the Ag⁰ catalyst for the next catalytic cycle [44]. TBHP serves as a source of reactive oxygen radicals (e.g., *t*-BuO[•]), which would act upon the benzyl alcohol to generate benzaldehyde in situ. Then in the next step benzaldehyde could convert to benzoic acid [31]. Our investigation implicated that the reaction proceeds via a radical mechanism as employing Na₂CO₃ or Et₃N as additives did not change product yield and also, the benzoic acid formation was suppressed in the presence of ascorbic acid.

3.3 Adsorption Studies

The prepared p(AMPS-Na⁺-*co*-VIm) hydrogel was employed as adsorbent for the adsorptive removal of benzyl alcohol, BA, from aqueous medium. Figure 6a and b illustrates variations in adsorption capacity of BA at 25 °C and 60 °C, respectively. As depicted in Fig. 6, the adsorption efficiency

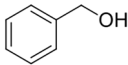
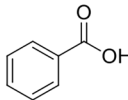
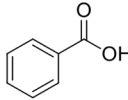
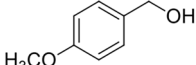
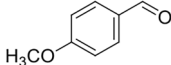
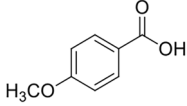
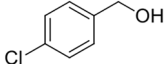
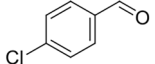
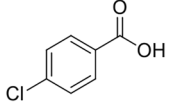
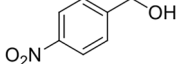
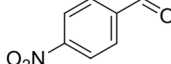
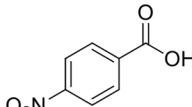
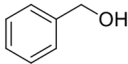
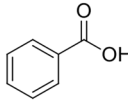
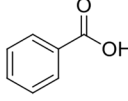
of the BA molecules on the hydrogel was enhanced with time. After six hours, this capacity achieved equilibrium. However, after this point, no considerable change in the adsorption capacity of the BA molecules was observed.

This molecule presents two active centers for the interaction with the surface: the π -system of the aromatic ring and the OH alcoholic group. Initially, $-\text{SO}_3$, $\text{CO}-\text{NH}^-$ and the imidazole functional groups in the hydrogel were ready to interact with benzyl alcohol via hydrogen bonding, π - π stacking and van der Waals forces [45–47]. During this

process, the BA molecules diffused on the hydrogel surface and saturated all the functional groups. Hence, the adsorption efficiency gradually decreased and approached the equilibrium.

Figure 7a depicts the impact of different amounts of p(AMPS- Na^+ -*co*-VIm) on the adsorption capacity of the BA molecules. As seen in Fig. 7a, with the increment of the amount of p(AMPS- Na^+ -*co*-VIm) hydrogel from 50 to 250 mg, the adsorption level of BA abruptly increased. The insertion of more hydrogel led to a gradual increase in

Table 4 Oxidation of benzylic alcohols by p(AMPS- H^+ -*co*-VIm)-Ag in the presence of O_2 /TBHP as oxidant

Entry	Substrate	Conversion ^a (%) TBHP/ O_2	Product	Selectivity (%) O_2 / TBHP
1		36.5/21		86/>99
				14/-
2		45/30		82/>99
				18/-
3		19/10		92/>99
				8/-
4		12/6.4		>99/>99
				-/-
5 ^b		12/18		>99/>99
				-/-

Catalyst (p(AMPS- H^+ -*co*-VIm)-Ag) contain 0.005 mmol H_2O (5 mL), Ag, substrate (1.0 mmol), temperature 60 °C, Time = 6 h,

^aConversions are based on the starting substrate

^bCatalyst {(p(AMPS- H^+)-Ag 0.005 mmol Ag)}

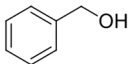
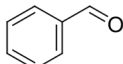
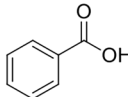
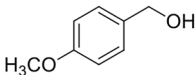
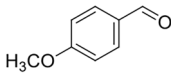
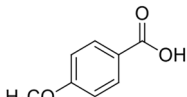
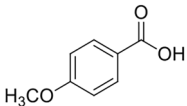
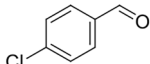
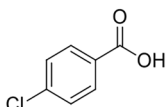
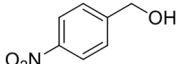
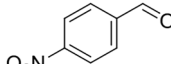
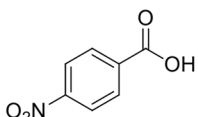
the adsorption capacity till the equilibrium was achieved. In detail, an increase in the volume of adsorbent boosted the surface area and the accessible adsorption sites on the hydrogel. Therefore, the accessible sites per unit mass increased [48].

Another contributing force to adsorption capacity is the concentration of adsorbate solutions. Considering this issue, this study also examined variations in the initial concentration of adsorbate solutions. As for BA, three initial concentrations (25, 50, and 100 ppm) were considered for the solution. So, three mixtures were prepared. The adsorbent was 250 mg of dried p(AMPS-Ag⁺-co-VIm) hydrogel added to 40 mL of each solution. Figure 7b reports the percent of BA adsorbed with respect to time intervals. With a boost in the concentration of the adsorbate mixture from 25 to 100 ppm, the amount of adsorbed BA was raised from 16% to 39%,

which indicates that the solution with a low concentration does not have the capability to saturate the active adsorption sites of the adsorbent. On the other hand, as the concentration of the adsorbate solution rose, the active adsorption sites were slowly filled with BA which proves the increment of adsorption efficiency.

The effect of Ag nanoparticles in the adsorption efficiency of the prepared hydrogel was also investigated. Equivalent amounts of the bare hydrogel and silver nanocomposite were added in aqueous solutions of BA. The adsorption capacity obtained are 39% and 46.5% for p(AMPS-Na⁺-co-VIm) hydrogel and p(AMPS-Na⁺-co-VIm)-Ag composite, respectively. The results indicated that a greater volume of BA was adsorbed on the p(AMPS-Na⁺-co-VIm)-Ag composite. Moreover, the Ag nanoparticles on the hydrogel had great surface energy; therefore, the BA molecules were easily

Table 5 Oxidation of benzylic alcohols in the presence of 1,4-BB-p(AMPS-Na⁺-co-VIm)-Ag

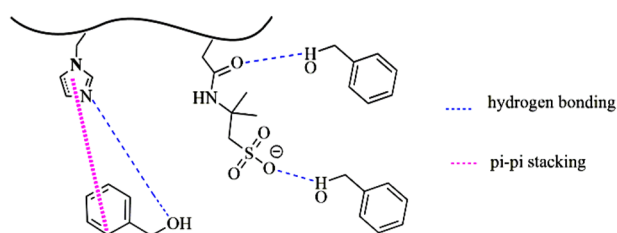
Entry	Substrate	Conversion ^a (%) TBHP/O ₂	Product	Selectivity (%) TBHP/ O ₂
1		84/72		60/83
				40/17
2		92/80		54/76
				46/24
3		51/42		63/82
				37/18
4		40/30		71/90
				29/10

Catalyst (p(AMPS-Na⁺-co-VIm)-BB-Ag), substrate (1.0 mmol), H₂O (5 mL), TBHP (1 mmol), temperature 60 °C, Time = 6 h

^aConversions are based on the starting substrate

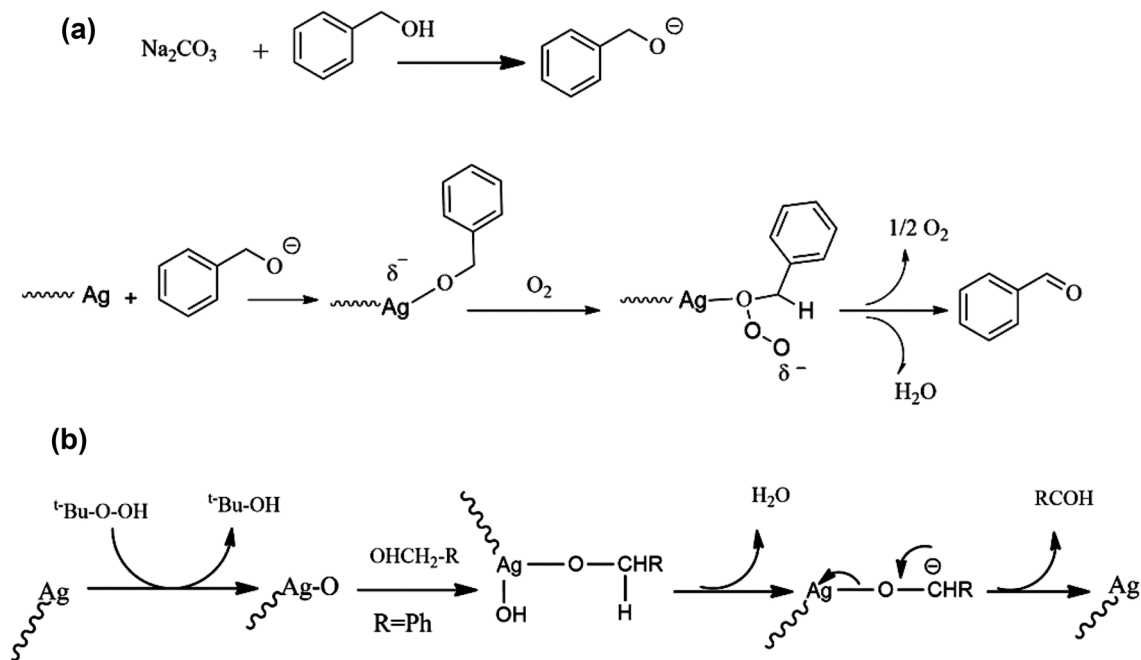
adsorbed by them. This phenomenon can be attributed to the greater binding affinity between the Ag nanoparticles and the BA molecules. Therefore, the fabrication of Ag nanoparticles in p(AMPS- Na^+ -*co*-VIm) hydrogel increases its adsorption capacity [49]. The number of active adsorption sites on the surface of the hydrogel was also raised owing to the augmentation of Ag nanoparticles, which elevated the adsorption efficiency of BA [50]. There are three possible explanations for an increase in BA uptake. The first one is the presence of silver nanoparticles on the backbone of the nanocomposite. These silver nanoparticles have a great tendency to interact with the BA molecules. The second one is associated with the thermal stability of the nanocomposite. In effect, the greater the number of Ag nanoparticles, the higher the thermal stability of the nanocomposite. The last one pertains to the formation of a highly crystalline nanocomposite owing to an increase in the number of Ag nanoparticles, which in turn promotes adsorption capacity [51].

There are also other factors contributing to the improvement of hydrogels adsorption property such as van der Waals, hydrogen bond, π - π stacking interaction, and hydrophobic interaction [52]. As shown in Fig. 8, the existence of these interactions is further confirmed by FTIR spectra of p(AMPS- Na^+ -*co*-VIm) after BA adsorption. Compared to that of p(AMPS- Na^+ -*co*-VIm) before adsorption, the peak of SO_3 groups of the hydrogel is shifted from 1051 to 1078 cm^{-1} after adsorption toward BA, which is owing to the hydrogen bonding between the SO_3 groups in AMPS- Na^+ and BA. Moreover, the H bond can also promote the



Scheme 3 Schematic interactions of BA onto the p(AMPS- Na^+ -*co*-VIm) hydrogel

adsorption and diffusion of the substrate. The carbonyl groups in the amide bond can adsorb benzyl alcohol through forming hydrogen bond between the oxygen atom and the hydroxyl group on the benzyl alcohol as the first step in Scheme 3 [53]. It is observed that the band of amide $\text{C}=\text{O}$ groups of the hydrogel is shifted from 1662 to 1668 cm^{-1} after adsorption toward BA. This is also because there are hydrogen bonding between MBA and AMPS- Na^+ segments and -OH group of BA [54]. There three peaks are witnessed about 1454 cm^{-1} , 1228 cm^{-1} and 1112 cm^{-1} assigned to CH_2 scissor bending vibration, the CH in-plane bending vibration and the C-O bond stretching vibration peak of benzylalcohol, respectively. It is worth noting that the characteristic C-O band of BA adsorbed on the p(AMPS- Na^+ -*co*-VIm) surface (1112 cm^{-1}) showed a blue shift compared to free BA molecule (1080 cm^{-1}). The results indicate that BA molecules can efficiently adsorb at p(AMPS- Na^+ -*co*-VIm). Besides, the signal at 3110 cm^{-1} for the stretching vibration



Scheme 2 Plausible pathways for the oxidation of alcohols in the presence of Ag-nanocomposites by **a** O_2 and **b** TBHP

of N–H should have been a sharp peak, but it became wider owing to the water absorption [55].

To compare the adsorption capacity of p(AMPS- Na^+ -*co*-VIm) hydrogels with p(AMPS- H^+ -*co*-VIm), the same amount of p(AMPS- H^+ -*co*-VIm) hydrogel as that of p(AMPS- Na^+ -*co*-VIm) hydrogel was inserted in the BA adsorption reactions. Because the pores of the p(AMPS- H^+ -*co*-VIm) hydrogel were smaller than those of the p(AMPS- Na^+ -*co*-VIm) hydrogel, the adsorption efficiency of BA was lower for the p(AMPS- H^+ -*co*-VIm) hydrogel. Therefore, the great adsorption efficiency of p(AMPS- Na^+ -*co*-VIm) hydrogels can be attributed to their favorable porous structure. The distribution of BA molecules and solvents in p(AMPS- Na^+ -*co*-VIm) pores is greater than that in p(AMPS- H^+ -*co*-VIm) pores. Consequently, active adsorption sites are less accessible in p(AMPS- H^+ -*co*-VIm) hydrogels than in p(AMPS- Na^+ -*co*-VIm) hydrogels. In the same way, p(AMPS- H^+ -*co*-VIm)-Ag compounds tend to have greater catalytic activity

than bare hydrogels p(AMPS- H^+ -*co*-VIm). The adsorption capacity was 28% and 34%, for p(AMPS- H^+ -*co*-VIm) and p(AMPS- H^+ -*co*-VIm)-Ag, respectively.

In the current study, the role of quaternizing p(AMPS- Na^+ -*co*-VIm) hydrogels in the adsorption behavior of BA was also examined. The same amount of the quaternized hydrogel was inserted in the aqueous solution of BA (100 ppm) at room temperature. The results revealed that the quaternized hydrogel yielded a greater adsorption capacity for BA (48%) than the non-quaternized hydrogel. It can be stated that the hydrophobicity and flexibility of the quaternized hydrogel enhanced in the aqueous solution, which improved π - π interactions among the aromatic compounds of VIm and BA and eventually increased the uptake of BA in this hydrogel. To be more precise, with an increment in the flexibility of alkyl chains, the imidazole groups easily rotated, which enhanced the possibility of π -type interactions between the

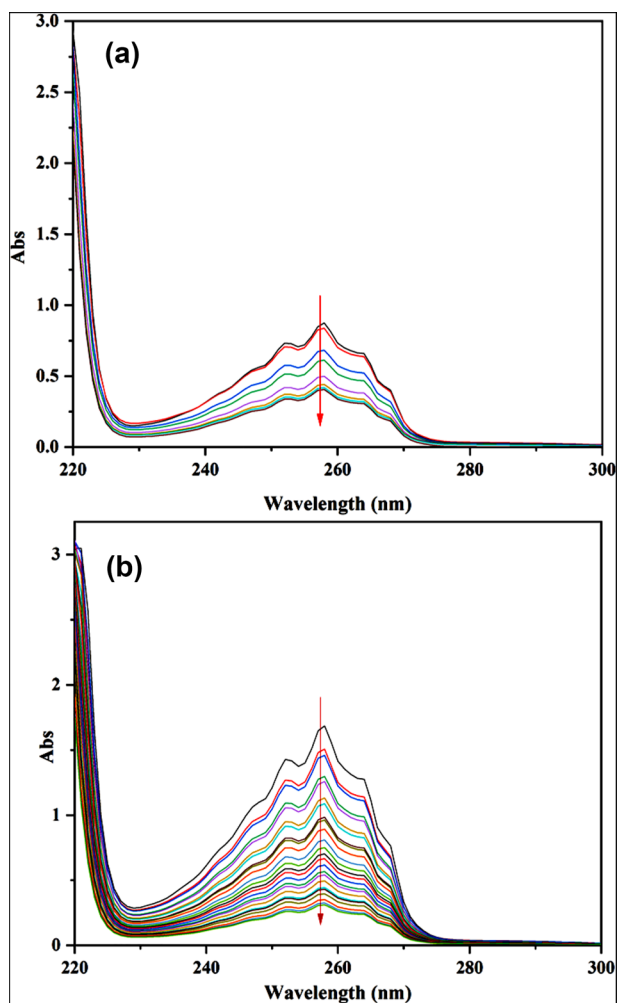


Fig. 6 UV-Vis spectrum of Benzyl alcohol adsorption by p(AMPS- Na^+ -*co*-VIm) at **a** 25 °C and **b** 60 °C

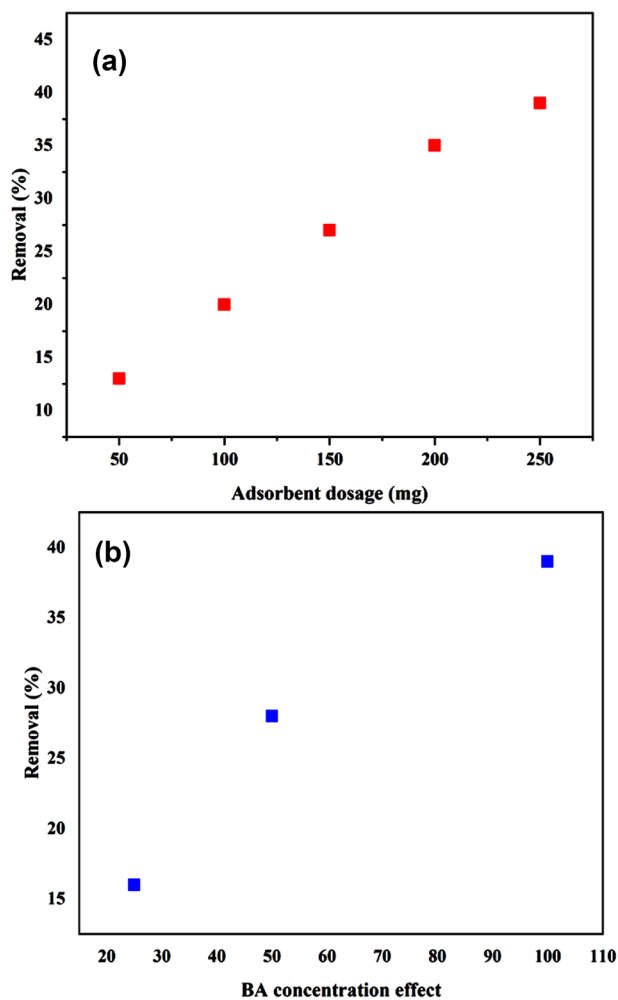


Fig. 7 **a** Effect of adsorbent dosage, **b** initial BA concentration effect on benzyl alcohol adsorption

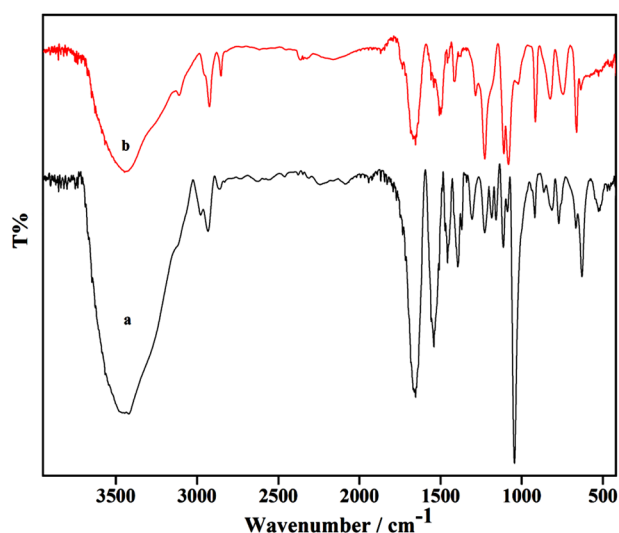


Fig. 8 FTIR spectra of (a) p(AMPS-NA⁺-co-VIm) and (b) p(AMPS-NA⁺-co-VIm)/BA

BA molecules and the imidazole ring. Other contributing factors to the adsorption behavior of BA on the surface of the quaternized hydrogel are as follows: the electron donor-electron acceptor interaction between OH^{-δ} and N⁺ in the quaternized hydrogel, anion- π interactions between Br⁻ and the aromatic ring of BA, H-bonding between CH₃ and O atoms, and CH- π interactions between alkyl chains and the aromatic ring of BA [55].

4 Conclusion

Diverse hydrogels synthesized by changing pH of reaction media, like neutral or basic, and related to the reaction condition, different behavior in terms of porosity, metal amount loading, dye removal and catalytic activity was observed for p(AMPS-Na⁺-co-VIm) and p(AMPS-H⁺-co-VIm) hydrogels. The catalytic efficiency of the catalysts was evaluated by catalytic oxidation of alcohols. Despite the fact that the hydrogels with high performance achieved at neutral condition, but their quality can be further enhanced using the quaternization technique. The results also indicate that compared to protonated imidazole in acidic media, protonated imidazole nitrogen with alkyl chains produces hydrogel-base catalysts that have greater catalytic activity, due to the flexibility of quaternized hydrogels in comparison to the other one. Notably, the higher removal efficiency of cationic dyes makes our ionogels complementary to other imidazolium based gels which these ion gels can display higher removal performance in the presence of anionic dyes. The attempt to correlate performance of hydrogel phases to their structural features highlights that morphology of materials plays a significant role in determining the adsorption ability. Above

all, these catalysts offer other benefits such as great recoverability, reusability, and stability.

The present study can contribute to the field by proposing a new way to construct beneficial and stable metal nanoparticle catalysts with numerous practical implications in wastewater treatment.

Acknowledgements The authors are grateful to the University of Zanjan for financial support of this study.

Declarations

Conflict of interest The authors declare that they have no conflict of interest.

References

1. Thakur S, Govenderv PP, Mamo MA, Tamulevicius S, Mishra YK, Thakur VK (2017) Progress in lignin hydrogels and nanocomposites for water purification: future perspectives. *Vacuum* 146:342–355
2. Olivera S, Muralidhara HB, Venkatesh K, Guna VK, Gopalakrishna K, Kumar Y (2016) Potential applications of cellulose and chitosan nanoparticles/composites in wastewater treatment: a review. *Carbohydr Polym* 153:600–618
3. Hamed H, Moradi S, Hudson SM, Tonelli AE (2018) Chitosan based hydrogels and their applications for drug delivery in wound dressings: a review. *Carbohydr Polym* 199:445–460
4. Caló E, Khutoryanskiy VV (2015) Biomedical applications of hydrogels: a review of patents and commercial products. *Eur Polym J* 65:252–267
5. Ullah F, Othman MBH, Javed F, Ahmad Z, Akil HM (2015) Classification, processing and application of hydrogels: a review. *Mater Sci Eng C* 57:414–433
6. Sahiner N, Yasar AO (2016) Co nanoparticle decorated magnetic core, polymeric ionic liquid shell composites for H₂ production. *Fuel Process Technol* 144:124–131
7. Wang Y, Guo L, Yin L (2019) Progress in the heterogeneous catalytic cyclization of CO₂ with epoxides using immobilized ionic liquids. *Catal Lett* 149:985–997
8. Demirci S, Zekoski T, Sahiner N (2019) The preparation and use of p (2-acrylamido-2-methyl-1-propanesulfonic acid)-tris (dioxo-3, 6-heptyl) amine (p (AMPS)-TDA-1) ionic liquid microgel in hydrogen production. *Polym Bull* 76:1717–1735
9. Nulwala H, Mirjafari A, Zhou X (2018) Ionic liquids and poly(ionic liquid)s for 3D printing a focused mini-review. *Eur Polym J* 108:390–398
10. Sahiner N, Yasar AO (2016) Imidazolium based polymeric ionic liquid microgels as an alternative catalyst to metal catalysts for H₂ generation from methanolysis of NaBH₄. *Fuel Process Technol* 152:316–324
11. Nguena CT, Kasi RM (2015) Nanocomposite hydrogels based on liquid crystalline brush-like block copolymer–Au nanorods and their application in H₂O₂ detection. *Chem Commun* 51:12174–12177
12. Marullo S, Rizzo C, Dintcheva NT, Giannici F, D’Anna F (2018) Ionic liquids gels: Soft materials for environmental remediation. *J Colloid Interface Sci* 517:182–193
13. Atta AM, Al-Lohedan HA, Ezzat AO, Tawfik AM, Hashem AI (2017) Synthesis of zinc oxide nanocomposites using poly

- (ionic liquids) based on quaternary ammonium acrylamidomethyl propane sulfonate for water treatment. *J Mol Liq* 236:38–47
14. Mittal H, Kumar V, Saruchi SS (2016) Adsorption of methyl violet from aqueous solution using gum xanthan/Fe₃O₄ based nanocomposite hydrogel. *Int J Biol Macromol* 89:1–11
 15. Bagheri Marandi G, Kermani ZP, Kurdtabar M (2013) Fast and efficient removal of cationic dyes from aqueous solution by collagen-based hydrogel nanocomposites. *Polym Plast Technol Eng* 52:310–318
 16. Kurdtabar M, Peyvand Kermani Z, Bagheri Marandi G (2015) Synthesis and characterization of collagen-based hydrogel nanocomposites for adsorption of Cd²⁺, Pb²⁺, methylene green and crystal violet. *Iran Polym J* 24:791–803
 17. Limparyoon N, Seetapan N, Kiatkamjornwong S (2011) Acrylamide/2-acrylamido-2-methylpropane sulfonic acid and associated sodium salt superabsorbent copolymer nanocomposites with mica as fire retardants. *Polym Degrad Stab* 96:1054–1063
 18. Odian G (2004) Principles of polymerization, 4th edn. Wiley, New Jersey
 19. Alejandra O, Emilio B, Guillermino B (2008) New Interpenetrating polymer networks of N-isopropylacrylamide/N-acryloxysuccinimide: synthesis and characterization. *Polym Bull* 60:515–524
 20. Lin SB, Yuan CH, Ke AR, Quan ZL (2008) Electrical response characterization of PVAcP(AA/AMPS) IPN hydrogels in aqueous Na₂SO₄ solution. *Sens Actuators B* 134:281–286
 21. Durmaz S, Okay O (2000) Acrylamide/2-acrylamido-2-methylpropane sulfonic acid sodium salt-based hydrogels: synthesis and characterization. *Polymer* 41:3693–3704
 22. Mohan A, Rout L, Thomas AM, Peter J, Nagappan S, Parambath S, Ha CS (2020) Palladium nanoparticles-anchored dual-responsive SBA-15-PNIPAM/PMAA nanoreactor: a novel heterogeneous catalyst for a green Suzuki-Miyaura crosscoupling reaction. *RSC Adv* 10:28193–28204
 23. Ma CY, Dou BJ, Li JJ, Cheng J, Hu Q, Hao ZP, Qiao SZ (2009) Catalytic oxidation of benzyl alcohol on Au or Au–Pd nanoparticles confined in mesoporous silica. *Appl Catal B Environ* 92:202–208
 24. Kim DH, Jo WH (2000) Studies on polymer–metal interfaces. 2. competitive adsorption between oxygen- and nitrogen-containing functionality in model copolymers onto metal surfaces. *Macromolecules* 33:3050–3058
 25. Kang ET, Neoh KG, Tan KL, Morikawa M, Uyama Y, Ikada Y (1992) Surface modifications polyaniline of films by graft copolymerization. *Macromolecules* 25:1959–1965
 26. Ma ZH, Han HS, Tan KL, Kang ET, Neoh KG (1999) Thermally induced surface graft copolymerization with concurrent lamination of polyaniline films under atmospheric conditions. *Int J Adhes Adhes* 19:359–365
 27. Liu K, Quin T, Sun Y, Hou C, Cao X, Jiang S (2018) Synergistic effect between Ag and Mn₃O₄ in the gas phase oxidation of alcohols. *Catal Commun* 113:15–18
 28. Jia L, Zhang S, Gu F, Ping Y, Guo X, Zhong Z, Su F (2012) Highly selective gas-phase oxidation of benzyl alcohol to benzaldehyde over silver containing hexagonal mesoporous silica. *Microporous Mesoporous Mater* 149:158–165
 29. Han SW, Kim Y, Kim K (1998) Dodecanethiol-derivatized Au/Ag bimetallic nanoparticles: TEM, UV/VIS, XPS, and FTIR analysis. *J Colloid Interface Sci* 208:227–228
 30. Genc F, Uzun C, Guven O (2016) Quaternized poly(1-vinylimidazole) hydrogel for anion adsorption. *Polym Bull* 73:179–190
 31. Azizi K, Esfandiary N, Karimi M, Yazdani E, Heydari A (2016) Imidazolium chloride immobilized on copper acetylacetonate-grafted magnetic chitosan as a new metal/ionic liquid bifunctional catalyst for selective oxidation of benzyl alcohols in water. *RSC Adv* 6:89313–89321
 32. Sharma PD, Panchariya P, Purohit P, Sharma P (2013) Structure-reactivity correlation in the oxidation of substituted benzyl alcohols by imidazolium fluorochromate. *Eur Chem Bull* 2:816–824
 33. Harada T, Ikeda S, Hashimoto F, Sakata T, Ikeue K, Torimoto T, Matsumura M (2010) Catalytic activity and regeneration property of a Pd nanoparticle encapsulated in a hollow porous carbon sphere for aerobic alcohol oxidation. *Langmuir* 26:17720–17725
 34. Narayanan S, Judithvijaya J, Sivasanker S, JohnKennedy L, Jesudoss SK (2015) Structural, morphological and catalytic investigations on hierarchical ZSM-5 zeolite hexagonal cubes by surfactant assisted hydrothermal method. *Powder Technol* 274:338–348
 35. Feng Y, Zeng A (2020) Selective liquid-phase oxidation of toluene with molecular oxygen catalyzed by Mn₃O₄ nanoparticles immobilized on CNTs under solvent-free conditions. *Catalysts* 10:623
 36. Santiago PHO, Aiube CM, de Macedo JL, Gatto CC (2020) Hydrazone-derived copper(II) coordination polymer as a selective liquid-phase catalyst: Synthesis, crystal structure and performance towards benzyl alcohol oxidation. *Mol Catal* 496:111177
 37. Cang R, Lu B, Li X, Niu R, Zhao J, Cai Q (2015) Iron-chloride Ionic liquid immobilized on SBA-15 for solvent-free oxidation of benzyl alcohol to benzaldehyde with H₂O₂. *Chem Eng Sci* 137:268–275
 38. Ghalavand N, Heravi MM, Nabid MR, Sadeghi R (2019) Preparation, characterization and application of core-shell Fe₃O₄@MAPTMS@PAA@Triazole@Cu(I) nano-composite as a magnetically separable and highly efficient catalyst for selective oxidation of aromatic alcohols using hydrogen peroxide. *J Alloys Compd* 799:279–287
 39. Ali SR, Bansal VK, Khan AA, Jain SK, Ansari MA (2009) Growth of zinc hexacyanoferrate nanocubes and their potential as heterogeneous catalyst for solvent-free oxidation of benzyl alcohol. *J Mol Catal A Chem* 303:60–64
 40. Deori K, Kalita C, Deka S (2015) (100) surface-exposed CeO₂ nanocubes as an efficient heterogeneous catalyst in the tandem oxidation of benzyl alcohol, para-chlorobenzyl alcohol and toluene to the corresponding aldehydes selectively. *J Mater Chem A* 3:6909–6920
 41. Hoorn JAA, Van Soolingen J, Versteeg GF (2005) Modelling toluene oxidation—incorporation of mass transfer phenomena. *Chem Eng Res Des* 83:187–195
 42. Abednatanzi S, Leus K, Derakhshandeh G, Nahra F, Keukeleere KD, Hecke KV, Driessche IV, Abbasi A, Nolan SP, Voort PVD (2017) POM@IL-MOFs—incclusion of POMs in ionic liquid modified MOFs to produce recyclable oxidation catalysts. *Catal Sci Technol* 7:1478–1487
 43. Doherty S, Knight JG, Carroll MA, Clemmet AR, Ellison JR, Backhouse T, Holmes N, Bourne RA (2016) Efficient and selective oxidation of sulfides in batch and continuous flow using styrene-based polymer immobilised ionic liquid phase supported peroxotungstates. *RSC Adv* 6:73118–73131
 44. Sarmah B, Srivastava R, Satpati B (2016) Highly efficient silver nanoparticles supported nanocrystalline zirconosilicate catalyst for the epoxidation and hydration reactions. *Chem Select* 5:1047–1056
 45. Rodriguez JL, Pastor E (2000) A comparative study on the adsorption of benzyl alcohol, toluene and benzene on platinum. *Electrochim Acta* 45:4279–4289
 46. Zhou YM, Zhang M, Hu XY, Wang XH, Niu JY, Ma TS (2013) Adsorption of cationic dyes on a cellulose-based multicarboxyl adsorbent. *J Chem Eng Data* 58:413–442
 47. Tang Y, He T, Liu Y, Zhou B, Yang R, Zhu L (2017) Sorption behavior of methylene blue and rhodamine B mixed dyes onto chitosan graft poly (acrylic acid-co-2-acrylamide-2-methyl propane sulfonic acid) hydrogel. *Adv Polym Technol* 37:2568–2578

48. Taghavi Nakhjiri M, Kurdtabar M (2019) Adsorption of methylene blue, brilliant green and rhodamine B from aqueous solution using collagen-g-p(AA-co-NVP)/Fe₃O₄@SiO₂ nanocomposite hydrogel. *J Polym Environ* 27:581–599
49. Zheng ALT, Phromsatit T, Boonyuen S, Andou Y (2020) Synthesis of silver nanoparticles/porphyrin/reduced graphene oxide hydrogel as dye adsorbent for wastewater treatment. *Flat Chem* 23:100174
50. Aboelfetoh EF, Gemeay AH, El-Sharkawy RG (2020) Effective disposal of methylene blue using green immobilized silver nanoparticles on graphene oxide and reduced graphene oxide sheets through one-pot synthesis. *Environ Monit Assess* 192:355
51. Salem MA, Elsharkawy RG, Hablas MF (2016) Adsorption of brilliant green dye by polyaniline/silver nanocomposite: kinetic, equilibrium, and thermodynamic studies. *Eur Polym J* 75:577–590
52. Yao G, Bi W, Liu H (2020) pH-responsive magnetic graphene oxide/poly(NVI-co-AA) hydrogel as an easily recyclable adsorbent for cationic and anionic dyes. *Colloids Surf A* 588:124393
53. Wang Q, Ge M, Dou Y, Yang F, Wang J, Shao Y, Huang A (2020) Engineering ultrafine Pd clusters on laminar polyamide: a promising catalyst for benzyl alcohol oxidation under air in water. *Mol Catal* 497:111203
54. Toledo PVO, Bernardilleni OD, Sabadini E, Petri DFS (2020) The states of water in tryptophan grafted hydroxypropyl methylcellulose hydrogels and their effect on the adsorption of methylene blue and rhodamine B. *Carbohydr Polym* 248:116765
55. Karimi-Maleh H, Ranjbari S, Tabhaei B, Ayati A, Orooji Y, Alizadeh M, Karimi F, Salmanpour S, Rouhi J, Sillanpaa M, Sen F (2021) Novel 1-butyl-3-methylimidazolium bromide impregnated chitosan hydrogel beads nanostructure as an efficient nanobio-adsorbent for cationic dye removal: kinetic study. *Environ Res* 195:110809

Publisher's Note Springer Nature remains neutral with regard to jurisdictional claims in published maps and institutional affiliations.